Annu. Rev. Fluid Mech. 2000. 32:613–657

FLUID MOTIONS IN THE PRESENCE OF STRONG STABLE STRATIFICATION

James J. Riley and Marie-Pascale Lelong
University of Washington, Seattle, Washington 98195; e-mail: rileyj@u.washington.edu
Northwest Research Associates, Bellevue, Washington 98040; e-mail: pascale@nwra.com

Key Words geophysical fluid mechanics, turbulence, rotation

■ **Abstract** We review the dynamics of stably stratified flows in the regime in which the Froude number is considered small and the Rossby number is of order one or greater. In particular we emphasize the nonpropagating component of the flow field, as opposed to the internal wave component. Examples of such flows range from the later stages of decay of turbulent flows to mesoscale meteorological flows. Results from theoretical analyses, laboratory experiments, and numerical simulations are presented. The limiting form of the equations of motion appears to describe the laboratory experiments and numerical simulations rather well. There are similarities with the dynamics of two-dimensional flows, but three-dimensional effects are clearly important. A number of remaining open issues are discussed.

1. INTRODUCTION

There are many instances in nature and technology in which flows are strongly affected by stable density stratification. For instance, propagating internal gravity waves owe their existence to the presence of a restoring buoyancy force, and turbulence, especially in its later stages of decay, can be dominated by the presence of a stabilizing stratification. In the atmosphere and oceans, flows on intermediate scales are usually strongly influenced by stable stratification; in these cases, the rotation of the earth is an important factor as well. In this review, we address the dynamics of flows that are strongly affected by stable density stratification. We do not address propagating internal waves, because this phenomenon has been treated at great length in many symposia, texts, and other formats; instead we address the nonpropagating component of the motion, the component that tends to have quasihorizontal motions and possesses potential vorticity.

For example, when turbulence is generated in the presence of stable density stratification, it often occurs locally and without a continuous source of energy. Examples of this are the local breakdown of propagating internal waves (e.g. Lelong & Dunkerton 1998a,b, Lombard & Riley 1996b, Orlanski & Bryan 1969)

0066–4189/00/0115–0613$12.00

or a local shear instability (e.g. Turner 1973). It is suspected, for example, that turbulence occurs sporadically throughout the oceans because of these mechanisms (Gregg 1987). This intermittent behavior is even expected to occur near boundaries under stably stratified conditions, as observed in the nocturnal atmospheric boundary layer (Mahrt 1998) and as predicted by direct numerical simulations (Barnard 1999). Such turbulence, although possibly initially very strong, will decay without a sustaining source of energy. At some point in its decay, the effect of density stratification will become important and even dominant.

The relative importance of density stratification for decaying turbulence is marked by a local Froude number, $F = u'/NL$, where u' is an rms turbulence velocity, L is a length scale of the energy-containing motions, and $N = [-(g/\rho)(d\rho/dz)]^{1/2}$ is the buoyancy frequency. Here $d\rho/dz < 0$ is the ambient density gradient. The Froude number can be considered as a measure of the relative importance of the buoyancy forces compared to the inertial forces. Local patches of turbulence often begin with a relatively large Froude number, indicating that inertial forces are dominating. As the turbulence decays, however, the Froude number decreases as u' decreases and L tends to grow, and the effects of stratification become important. At some point, as the buoyancy forces become of the order of the inertial forces, then $F \sim 1$. As the turbulence decays further, F may become small, and the stratification dominates the flow. It is this regime that is addressed in this review.

A vivid example of this process was reported in an earlier article in this series by Lin & Pao (1979). In their experiment, turbulence was generated by towing an axisymmetric model horizontally through a long tank filled with water. Without density stratification, the wake of the model behaved in the classical manner. When stable salt stratification was added to the water and the experiment was repeated, the near-field wake, in which F was rather large, remained approximately the same as in previous, nonstratified experiments. In the far field, as the wake turbulence decayed, F became small and buoyancy forces became dominant, and the behavior of the wake changed dramatically. The wake appeared to consist of quasihorizontal motions, reminiscent of a two-dimensional wake, but undulating in a sea of internal waves (see Figure 1). These quasihorizontal motions appeared to have considerable vertical structure.

The quasihorizontal motions observed by Lin & Pao (1979) are an example of the nonpropagating component of flow in the low-Froude-number regime. As we describe below, such motions range from simpler monopoles and dipoles to flows having complex horizontal and vertical structure. Various terminology has been used to designate these flows. Low-Froude-number flows with more complex structure behave differently than classical turbulence, and are strongly affected by the stable density stratification; therefore Lilly (1983) referred to these phenomena as stratified turbulence. These flows are sometimes referred to as vortical modes in the oceanographic literature (Müller et al 1986). In this review, we usually refer to this nonpropagating component of the flow as the *PV* component or, sometimes, the *PV* modes, because this component can be defined

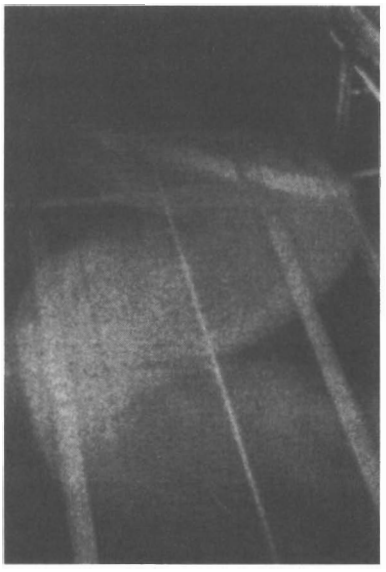

Figure 1 Top view of dye visualization of a late wake; $Nt = 37.6$ (Lin & Pao 1979).

strictly in terms of the potential vorticity of the flow. (See Section 3.1 below.) This is to distinguish it from the internal-wave component, which possesses no potential vorticity.

When effects of system rotation are added to the stratification, such as would be the case for larger-scale flows in the atmosphere or oceans, then additional features occur. The importance of the effect of rotation can be measured by the Rossby number, defined here as $Ro = u'/fL$, where f is half the system rotation rate. (We consider only horizontal length scales small enough that f is approximately constant, that is, the f-plane approximation.) When the Rossby number is large, the effects of rotation tend to be weak. For $Ro \sim 1$, however, rotational effects become important, and the flow field is significantly modified. For example, rotation tends to suppress vertical variability (Proudman 1916, Taylor 1923), a potentially important feature of strongly stratified flows, and to modify the behavior of propagating internal waves. As the Rossby number becomes small at the same time as the Froude number is small, the flow enters into the quasi-geostrophic (QG) regime, studied extensively in the past. In this review, we emphasize only the regimes with $Ro \geq O(1)$.

Other parameters are also expected to be important in describing turbulence with stable stratification. For example, the overturning length scale $L_0 = (\varepsilon/N^3)^{1/2}$, defined independently by Dougherty (1961), Lumley (1964), and Ozmidov (1965), is an estimate of the largest scale of the turbulence at which overturning can occur. Here ε is the kinetic energy dissipation rate. Note that, using the high Reynolds number scaling $\varepsilon \sim u'^3/L$, then $L_0/L \sim F^{3/2}$. The ratio of this overturning scale to the Kolmogorov scale, $L_k = (\nu^3/\varepsilon)^{1/4}$, is $(\varepsilon^3/\nu N^2)^{3/4}$. It is

thought that, when this ratio becomes of order 1, turbulence in the classical, three-dimensional sense is extinguished (Stillinger et al 1983); however, the existence of a critical value for this parameter has been questioned (Huq & Stretch 1995). Note that, again using high Reynolds number scaling, $\varepsilon/\nu N^2 \sim F^2 R_L$, where $R_L = u'L/\nu$ is a Reynolds number. Therefore, $\varepsilon/\nu N^2 \sim 1$ corresponds to $R_L \sim F^{-2}$. We will see below from laboratory studies and numerical simulations that, while $\varepsilon/\nu N^2$ may become very small, interesting and important motions may still exist.

The regime of stable stratification and weak rotation is of great importance in geophysical fluid dynamics, because it describes motions in the transition region between the large, energetic scales and the small scales at which energy is dissipated.

In the atmosphere, this is the mesoscale regime, with typical timescales ranging from the buoyancy period to the inertial period; associated nondimensional parameters are $F \leq O(1)$, $Ro \geq O(1)$. In this regime, quasihorizontal turbulent strata, reminiscent of the late stages of decaying, stratified turbulence in the laboratory, are often observed alongside internal waves. Gage (1979) proposed that the observed $-5/3$ horizontal kinetic energy spectrum at the mesoscale could be produced by an upscale transfer of energy through stratified turbulence from small-scale sources. Such behavior is characteristic of forced two-dimensional turbulence (Kraichnan 1967) and quasi-geostrophic turbulence (Charney 1971, Herring 1980). Lilly (1983) suggested that decaying convective clouds and thunderstorm anvil outflows could provide the sources at the small scales. Van Zandt (1982), on the other hand, has remarked that a similar spectrum in the ocean is generally attributed to wave processes (e.g. Garrett & Munk 1979) and has suggested that intermittent internal wave breaking will lead to saturated wave spectra with the observed spectral slope. Recent analysis of horizontal spectra for winds, temperature and trace gases over the Pacific Ocean suggests that stratified turbulence may be more prevalent than internal waves over the ocean (Cho et al, 1999). It is not known, at this point, whether waves or stratified turbulence dominate the atmospheric mesoscale signal; in retrospect, it appears likely that both types of motion are important.

The ability to distinguish between "fast" waves and "slow" turbulence may be important in resolving a related question concerning the existence and utility of the slow manifold for mesoscale motions. The notion of a slow manifold was introduced to describe the evolution of large-scale, "balanced" geophysical flows on a hypothetical manifold devoid of high-frequency "unbalanced" internal waves (Leith 1980, Lorenz 1980). For large-scale flows, the concept is justified by the very large temporal scale separation that makes it unlikely that the waves will interact significantly with the balanced flow. Because of this, and for numerical reasons as well, numerical weather forecasting models are typically initialized with raw atmospheric data that have been projected onto the slow manifold. Although, mathematically speaking, the concept of a slow manifold extends down to small-scale motions, it becomes unclear whether it remains useful for describ-

ing balanced flow evolution at small scales. On these scales, as we show in Section 3, there is now the possibility that balanced and unbalanced components will interact and exchange significant amounts of energy. Therefore, an initially balanced flow may not remain on the slow manifold. As weather forecasting models resolve finer and finer features, questions regarding the stability of the slow manifold must be resolved.

In the ocean, motions with scales that range from a few millimeters up to a few kilometers in the horizontal and up to a few hundred meters in the vertical are traditionally ascribed to internal waves and three-dimensional turbulence. That there might be some other types of motion at the oceanic small scale was first suggested during the analysis of the IWEX (Internal Wave Experiment) conducted in the late 1970's. The observed coherence in the vertical and the kinetic-to-potential energy ratio were found to be inconsistent with linear internal-wave theory in the fine-structure regime, defined as having vertical wavelengths ≤ 10 m (Briscoe 1975, Eriksen 1978, Müller et al 1978). Because of the inherent difficulties involved in measuring potential vorticity at small scales, internal wave and *PV* component signals are not easily distinguished (Müller et al 1988). For example, Doppler-shifted near-inertial waves viewed in a non-Lagrangian frame of reference may exhibit frequencies well below the Coriolis frequency, a characteristic also associated with the nonpropagating *PV* component (Kunze et al 1990). Moreover, in observations at very small scales, small signal-to-noise ratios are often encountered, making it difficult to differentiate *PV* component motions from ambient noise. Consequently, most of the present knowledge of the *PV* component in the open ocean remains largely speculative, having been inferred from a growing number of observations that cannot be explained with linear wave dynamics, and from the overriding evidence that stratified turbulence emerges in a variety of flows in which, as in the ocean thermocline, the dynamics are strongly influenced by the presence of a stabilizing vertical density gradient.

Perhaps the most compelling indirect evidence for the existence of small-scale *PV* component flow in the open ocean has come from the North Atlantic Tracer Release Experiment (NATRE) designed to accurately measure diapycnal and isopycnal diffusivities in the thermocline by examining the dispersion of an ocean tracer (Ledwell et al 1993). The observed cross-streak pattern suggests the presence of an efficient dispersion process at horizontal scales of 1 to 10 km and vertical scales of a few tens of meters. The oscillatory shear associated with internal waves on those scales cannot produce the observed dispersion pattern; it is, therefore, speculated that stratified turbulence, with its characteristic low-frequency shear, may be present (M-P Lelong, unpublished results 1999; Sundermeyer 1998).

Near seamounts, islands, and other topographic features, an important generation mechanism for smaller-scale *PV* motions is undoubtedly vortex shedding (Etling 1989, Kunze 1993, Kunze & Sanford 1993, Smith 1989, Smolarkiewicz & Rotunno 1989) and other interations with boundaries (e.g. Ahlnas et al 1987, Federov & Ginsburg 1989). For example, Smolarkiewicz & Rotunno performed

inviscid numerical simulations of low-Froude-number flows past three-dimensional obstacles and reported the formation of pairs of counterrotating, vertically oriented vortices on the lee side of the obstacle for $F \leq 0.5$. They interpret the presence of the vortices in terms of Ertel's potential vorticity conservation. Smith (1989) questions this interpretation and offers an alternate explanation based on the presence of a stagnation point and the ensuing flow bifurcations.

In both the atmosphere and ocean, a good understanding of the dynamics of strongly stratified flows as a function of ambient rotation is crucial to the development of accurate subgrid-scale parameterizations needed in large-scale general circulation models. For instance, to correctly model the effect of small, unresolved motions on the energy-carrying scales, we need to know the parameter ranges over which energy cascades upscale and downscale. Several studies have demonstrated the sensitivity of general circulation numerical models to the choice of diffusivity parameterizations (e.g. Bryan 1986, 1987; Chen & Young 1995, Cummins et al 1990). In the future, coupled ocean-atmosphere models that are used to address issues related to global climate change will rely on such parameterizations.

In the next section, we discuss some limiting conditions in the equations of motion as $F \to 0$, as well as some of the theoretical and mathematical ramifications of these conditions. In Section 3, we present some mathematical analyses of low-Froude-number regimes. In Section 4, we review various laboratory experiments that lend considerable insight into the dynamics of strongly stratified flows, and then in Section 5, we describe several numerical experiments designed to understand various aspects of these flows. Finally, in Section 6, we discuss some of the unresolved issues related to strongly stratified flows. Note that a number of other review articles have addressed related material. For example, in addition to the review of Lin & Pao (1979), Fernando (1991) has addressed turbulent mixing in stratified fluids, Gregg (1987) has reviewed turbulent mixing in the ocean, Hopfinger (1987) has reviewed the general topic of turbulence in stratified fluids, and Müller et al (1986) have reviewed a number of theoretical issues related to strongly stratified flows.

2. DECOMPOSITION OF MOTION AT LOW FROUDE NUMBER

2.1 Scaling Arguments

The dynamics of stratified turbulence can be understood by considering some simple scaling arguments and by using the fact that the Froude number F is small. Considering first internal waves, we choose the following scaling analysis:

$$\vec{x}_H \sim L_H,\ z \sim L_V$$

$$\vec{u}_H \sim u'$$

$$t \sim N^{-1} \frac{L_H}{L_V} = N^{-1} \alpha^{-1}.$$

Here the subscript H denotes the horizontal component of a vector, L_H and L_V are typical horizontal and vertical length scales, respectively, and α is the aspect ratio L_V/L_H. Gravity and the effective system rotation vectors are taken along the z-direction, and we use the notation

$$\vec{u} = (\vec{u}_H,\ w),\ \vec{x} = (\vec{x}_H,\ z),$$

where $\vec{x}$ is measured in the rotating frame of reference and $\vec{u}$ is the corresponding relative velocity. In scaling time, it is assumed that

$$\frac{f}{N} < \alpha \leq 1.$$

The pressure scaling is determined by assuming that the time derivative and pressure force terms in the horizontal momentum equation are of the same order, giving

$$p \sim \rho_o u'^2 F^{-1}.$$

Here, ρ_o is the (constant) average density, and the Froude number is now defined as

$$F = \frac{u'}{NL_V}.$$

The perturbation density scaling is obtained by assuming that the hydrostatic-balance terms in the vertical-momentum equation are of the same order, leading to

$$\rho \sim \rho_o \frac{u'^2}{gL_V} F^{-1}.$$

Finally, the scaling for the vertical velocity w is obtained by assuming that the time derivative term and the leading linear term in the density perturbation equation are of the same order, giving

$$w \sim \alpha u'.$$

Assuming the Navier-Stokes equations hold to within the Boussinesq approximation (see, e.g. Phillips 1966) and employing the above scaling gives, in non-dimensional form:

$$\frac{\partial}{\partial t}\vec{u}_H + F\left(\vec{u}_H \cdot \nabla\vec{u}_H + w\frac{\partial}{\partial z}\vec{u}_H\right) + \frac{1}{\alpha}\frac{f}{N}\vec{e}_z \times \vec{u}_H$$
$$= -\nabla_H p + \alpha^2 \frac{F}{R_L}\nabla^2\vec{u}_H \tag{1a}$$

$$\alpha^2\left(\frac{\partial w}{\partial t} + F\vec{u}_H \cdot \nabla w + \alpha F w\frac{\partial w}{\partial z}\right) = -\frac{\partial p}{\partial z} - \rho + \frac{F}{R_L}\nabla^2 w \tag{1b}$$

$$\nabla \cdot \vec{u}_H + \frac{\partial w}{\partial z} = 0 \tag{1c}$$

$$\frac{\partial \rho}{\partial t} + F\vec{u}_H \cdot \nabla\rho + \alpha^2 F w\frac{\partial \rho}{\partial z} - w = \frac{1}{\alpha^2}\frac{F}{R_L Sc}\nabla^2\rho \tag{1d}$$

Here ρ is the nondimensional density fluctuation about the ambient density; we have assumed, for simplicity, that the ambient density gradient is uniform (in z), and we have taken $\vec{e}_z$ to be the unit vector in the positive z-direction (opposite in direction to the force of gravity). The parameter $Sc = \nu/\mathcal{D}$ is the Schmidt number, where ν is the kinematic viscosity and $\mathcal{D}$ the molecular diffusivity of the diffusive medium, usually either salt or heat (internal energy).

In the limit as $F \to 0$, these equations linearize. Linear internal wave theory and weakly nonlinear theories can be developed from these equations, using perturbative methods (Müller et al 1986, Phillips 1966). Furthermore, simplifications can be obtained in the hydrostatic limit ($\alpha \to 0$ but $\alpha \geq N/f$). These equations do not, however, exhibit the properties of the *PV* component in this limit.

To address the dynamics of the *PV* component, following Riley et al (1981), we rescale the equations as follows. As above, we choose

$$\vec{x}_H \sim L_H,\ z \sim L_V$$

$$\vec{u}_H \sim u'.$$

The scaling for time is now chosen as an advective time scale, i.e.

$$t \sim L_H/u' = \alpha^{-1}N^{-1}F^{-1},$$

and the scaling for pressure is chosen so that the horizontal pressure gradient is of the same order as the nonlinear advective terms, i.e.

$$p \sim \rho_o u'^2.$$

To scale the perturbation density, approximate hydrostatic balance is assumed, giving

$$\rho \sim \rho_o \frac{u'^2}{L_V g}.$$

Finally, the scaling for the vertical velocity w is obtained by again assuming that the time derivative and leading linear terms in the perturbation density equation are of the same order, giving $w = u'\alpha F^2$. Note that, from this scaling for w, we expect the vertical velocity to be small, as observed in laboratory experiments.

Employing this scaling in the Navier-Stokes equations with the Boussinesq approximation gives the following nondimensional equations:

$$\frac{\partial}{\partial t}\vec{u}_H + \vec{u}_H \cdot \nabla\vec{u}_H + F^2 w \frac{\partial}{\partial z}\vec{u}_H + \frac{1}{Ro}\vec{e}_z \times \vec{u}_H = -\nabla_H p + \frac{1}{\alpha^2}\frac{1}{R_L}\nabla^2\vec{u}_H \tag{2a}$$

$$\nabla_H \cdot \vec{u}_H + F^2 \frac{\partial w}{\partial z} = 0 \tag{2b}$$

$$\alpha^2 F^2 \left[\frac{\partial w}{\partial t} + \vec{u}_H \cdot \nabla w + F^2 w \frac{\partial w}{\partial z}\right] = -\frac{\partial p}{\partial z} - \rho + \frac{F^2}{R_L}\nabla^2 w \tag{2c}$$

$$\frac{\partial \rho}{\partial t} + \vec{u}_H \cdot \nabla\rho + F^2 w \frac{\partial \rho}{\partial z} - w = \frac{1}{\alpha^2}\frac{1}{ScR_L}\nabla^2\rho. \tag{2d}$$

For $F \to 0$, $Ro \geq 1$, these equations reduce to the stratified turbulence (PV component) equations:

$$\frac{\partial}{\partial t}\vec{u}_H + \vec{u}_H \cdot \nabla\vec{u}_H + \frac{1}{Ro}\vec{e}_z \times \vec{u}_H = -\nabla_H p + \frac{1}{\alpha^2}\frac{1}{R_L}\nabla^2\vec{u}_H \tag{3a}$$

$$\nabla_H \cdot \vec{u}_H = 0 \tag{3b}$$

$$0 = -\frac{\partial p}{\partial z} - \rho \tag{3c}$$

$$\frac{\partial \rho}{\partial t} + \vec{u}_H \cdot \nabla\rho - w = \frac{1}{\alpha^2}\frac{1}{ScR_L}\nabla^2\rho. \tag{3d}$$

(See Embid & Majda 1996 for a rigorous mathematical derivation of these equations.) In theory, assuming that the initial conditions and boundary conditions are consistent with the scaling arguments, Equations 3a and 3b can be solved independently of the others to obtain $(\vec{u}_H, p)$. Then Equation 3c can be used to obtain ρ, and finally w can be obtained from 3d. This procedure is very similar to that introduced by Drazin (1961) for large-scale atmospheric flows in the presence of

strong, stable density stratification, which was extended and compared with laboratory data by Lilly (1973) and Riley et al (1976) for the case with no rotation ($Ro \to \infty$).

Note that Equations 3c and 3d suggest that vertical pressure gradients caused by differential horizontal motions will induce vertical displacements and velocities. This suggests that the *PV* component may radiate internal waves. Also note the difference in the propagation characteristics of the internal waves and the *PV* component. The internal waves are free to propagate to significant distances. The equations for the *PV* component, however, do not admit propagating solutions; therefore, a *PV* component region can only grow by advection and molecular diffusion.

Equations 3a and 3b, without rotation, appear to describe many of the features of strongly stratified flows observed in the laboratory, as we see in Section 4. Furthermore, they exhibit a number of very interesting characteristics. First, unlike the lowest-order equations obtained from the internal wave scaling, these lowest-order equations are nonlinear. Second, although in form Equations 3a and 3b appear to describe a two-dimensional flow, the equations do admit solutions that vary in three dimensions. The horizontal velocity field in each horizontal layer is coupled in the vertical direction through the diffusion term, whereas density and vertical velocity are coupled through the pressure term.

Lilly (1983) suggested that, for higher Reynolds number flows, the flow fields in adjacent horizontal layers would tend to decouple, leading to shear instabilities and smaller-scale turbulence. It is possible then that smaller-scale turbulence, and not molecular diffusion, would determine the approximate vertical length scale for these motions. We see in the later sections that the vertical shearing of horizontal currents can be a key feature of these flow fields.

Note that, for these lowest-order equations, the equation for the vertical vorticity ω_z is

$$\frac{\partial}{\partial t}\omega_z + \vec{u}_H \cdot \nabla\omega_z = \frac{1}{\alpha^2}\frac{1}{R_L}\nabla^2\omega_z.$$

Therefore, in the absence of molecular diffusion, the vertical vorticity following a fluid element is conserved, as in a two-dimensional flow; again note, however, that the flow is in general not two-dimensional. Furthermore, the equation for the horizontal vorticity vector $\vec{\omega}_H$ is

$$\frac{\partial}{\partial t}\vec{\omega}_H + \vec{u}_H \cdot \nabla\vec{\omega}_H - \frac{1}{Ro}\frac{\partial}{\partial z}\vec{u}_H = \vec{\omega} \cdot \nabla\vec{u}_H - \nabla \times (\rho\vec{e}_z) + \frac{1}{\alpha^2}\frac{1}{R_L}\nabla^2\vec{\omega}_H.$$

To the lowest order,

$$\vec{\omega}_H = \left(-\frac{\partial u_2}{\partial x_3}, \frac{\partial u_1}{\partial x_3}\right).$$

(Note that x_3 and z are used interchangeably, as are the subscripts z and 3.) Fur-

thermore, for example, in the equation for ω_1, one vortex stretching term, $\partial u_1/\partial x_1\ \partial u_2/\partial x_3$, one turning term, $-\partial u_1/\partial x_3\ \partial u_1/\partial x_2$, and one baroclinic term, $-\partial\rho/\partial x_2$, survive.

As pointed out by Riley et al (1981) and Lilly (1983), the solutions to this system of equations can be expressed in terms of a stream function $\psi(\vec{x}_H, z, t)$ as

$$\vec{u}_{pv} = \vec{e}_z \times \nabla_H \psi,$$

or, equivalently, in Fourier space as

$$\hat{\vec{u}}_{pv} = i(\vec{e}_z \times \vec{\kappa})\hat{\psi},$$

where $\hat{(\ )}$ denotes a Fourier transform and $\vec{\kappa}$ is the wave number vector. Using similar reasoning for the wave-scaled equations, 1a to 1d, with $F \to 0$, a velocity potential ϕ can be defined, giving the internal wave velocity as

$$\vec{u}_{iw} = \nabla_H \phi - \vec{e}_z \int \nabla_H^2 \phi\, dz.$$

The equivalent Fourier-space expression is

$$\hat{\vec{u}}_{iw} = i\,\vec{\kappa}_H \hat{\phi} + i\vec{e}_z \frac{\kappa_H^2}{\kappa} \hat{\phi},$$

with, for example, $\kappa = |\vec{\kappa}|$.

Lilly (1983) and McWilliams (1985) extended this scaling analysis to quasigeostrophic flows by considering the conditions $Ro \sim F \ll 1$. Lilly showed that Charney's (1971) theory for geostrophic turbulence could then be obtained. McWilliams considered the above scaling and the quasigeostrophic scaling in the context of the balanced equations (Lorenz 1960), and proved that the scaling for $F \to 0$ was valid uniformly in Ro.

2.2 Other Theoretical Approaches

In developing the concept of fossil turbulence, Gibson has addressed the later stages of decay of a turbulent region in a stratified fluid (e.g. Gibson 1980, 1987). His ideas have been very useful, for example, in interpreting data from laboratory (e.g. Ivey & Imberger 1991, Stillinger et al 1983) and field experiments (Imberger & Ivey 1991). Related to the concept of fossil turbulence are comments made regarding the sampling rates for highly intermittent turbulent events in the ocean.

By fossil turbulence Gibson means "a remnant fluctuation in any hydrophysical field produced by active turbulence which persists after the fluid is no longer actively turbulent (overturning) at the scale of the fluctuation" (Gibson 1987, p. 5383). This definition would include the *PV* component discussed in the previous section. Gibson, however, goes on to say that "fossil vorticity turbulence means an internal wave field produced when active turbulence is damped by buoyancy . . . the inertial forces at the scale of the fluctuations are smaller than the buoyancy

or viscous forces" (Gibson 1987, p. 5383). This would appear to preclude the concept of *PV* component developed in the previous section, both because the *PV* component does not consist of internal waves and also because inertial forces can be a principal feature.

Gibson defines several regimes in the transition of a turbulent patch into fossil turbulence. Early in the development of the turbulent region, when none of the scales of motion are dominated by buoyancy, the flow is labeled active. When the overturning scale becomes of the order of the turbulent integral scale (i.e. the local Froude number is of order one as in the discussion in the Introduction), Gibson concludes that "the largest scales of turbulence have been converted to internal waves . . . Only small-scale patches within the fossil microstructure are overturning and actively turbulent" (Gibson 1987, p. 5386). Gibson calls this the active/fossil turbulence regime. Although the beginning of this regime corresponds to the time of collapse in the three-dimensional flow to be discussed in regard to laboratory experiments in Section 4, it again does not allow for *PV* component in the largest scales. When the turbulence has decayed to the point where the overturning scale equals the Kolmogorov scale, i.e., from the Introduction, $(\varepsilon/\nu N^2) \sim 1$, Gibson concludes that no overturning can exist at any scale, and "complete fossilization" has occurred. Again, although these are very important and useful concepts, they do not address the *PV* component, a phenomenon that explains some of the laboratory and numerical experiments and geophysical data.

Using mathematical analysis, Pearson & Linden (1983) examined the final period of decay of a turbulent patch in a stratified fluid. They linearized the governing equations (arguing that the internal Reynolds number would be very small), used Fourier analysis, and sought the most slowly decaying solutions. They assumed that these slowly decaying modes would dominate at late times. For $Sc \gg 1$, as for salt dissolved in water, they obtained a slowly decaying mode consisting of mainly horizontal motion with small vertical length scale. The mode slowly decays because of convection, driven by potential energy stored in the perturbed density field and also by molecular diffusion, at a rate of approximately

$$\sigma \propto Sc^{-2/3} \left(\frac{\nu N^2}{L^2}\right)^{1/3},$$

where L is a measure of the size of the turbulent region. Comparisons of their theory with experiments gave rough agreement.

Their analysis excluded the *PV* component modes. Therefore it cannot describe, for example, some of the principal features of the laboratory experiments to be presented in Section 4. It is possible, however, that this mechanism is important in the very late stages of decay in these experiments, as the density field continues to restratify. In addition, the solution appears to address the regime Gibson refers to as complete fossilization.

3. MATHEMATICAL ANALYSIS

3.1 Flow Field Decomposition in Terms of Ertel's Potential Vorticity

Generally speaking, the dynamical distinction between wave and nonpropagating components can be made in terms of Ertel's potential vorticity Π (Ertel 1942). Potential vorticity has long been employed as a diagnostic tracer in large-scale geophysical flows, but its utility at small scales has only recently been recognized (Müller et al 1986). Considering a flow in a rotating reference frame and satisfying the Navier-Stokes equations subject to the Boussinesq approximation, Π is commonly defined as

$$\Pi \equiv \frac{(\vec{\omega} + f\vec{e}_z) \cdot \nabla\tilde{\rho}}{\rho_0}, \tag{4}$$

where $\vec{\omega}$ is measured in the rotating reference frame, and $\tilde{\rho}$ is the total density. From the governing equations, it is straightforward to establish that Π obeys the following equation

$$\frac{D\Pi}{Dt} = \nu\nabla^2\vec{\omega} \cdot \nabla\tilde{\rho} + \mathfrak{D}\nabla^2[\nabla\rho \cdot (\vec{\omega} + f\vec{e}_z)], \tag{5}$$

where the D/Dt is the material derivative. Therefore, in the absence of viscous and diffusive effects, Π is conserved along fluid-parcel trajectories (Pedlosky 1987). Thus, it does not propagate but is merely advected by the flow. We shall see later in this section that the conservation of potential vorticity exerts a strong constraint on the flow evolution.

The nonpropagating nature of Π suggests the following delineation between waves and nonpropagating motions: The wave field is defined to be precisely that part of the flow that propagates and hence does not contribute to the potential vorticity. The nonpropagating component, on the other hand, accounts for all of the potential vorticity of the flow. This latter nonpropagating component can, in theory, be split into a part that contains potential vorticity and a part that does not. We refer to the former as the *PV* component; we do not consider the latter in this review.

Physically, Π represents the vector component of the total vorticity (relative + planetary) perpendicular to isopycnal surfaces. When the deviations from equilibrium are slight, the isopycnal surfaces are, to a first approximation, horizontal. In the absence of rotation, the potential vorticity is then simply proportional to the vertical component of vorticity.

The correspondence between potential and vertical vorticities justifies the linear splitting of the velocity field introduced by Riley et al (1981) and Lilly (1983), described in Section 2.1:

$$\vec{u} = \{\nabla_H \phi + w\vec{e}_z\} + \vec{e}_z \times \nabla_H \psi. \tag{6}$$

The first bracketed term represents the wave and the second term the *PV* component.

Staquet & Riley (1989b) generalized the nonrotating linear wave/*PV* decomposition (which is only valid in the limit of very small density perturbations) to an exact decomposition by postulating a set of equations in an isopycnal coordinate frame. This generalized decomposition enables a diagnostic separation of the *PV* from the wave component for strongly nonlinear flows as long as the isopycnal surfaces remain single-valued, i.e. as long as they do not exhibit overturning.

3.2 Normal-Mode Decomposition

The dynamical decomposition of the velocity field, Equation 6, is most useful when $f = 0$. When $f \neq 0$, Π is no longer proportional to the vertical vorticity but includes an additional term. In this case, the distinction between the wave and *PV* components is most easily made in terms of the eigenvectors of the equations of motion linearized about a state of rest. Assuming $\kappa_z \neq 0$ and $\vec{\kappa}_H \neq \vec{0}$, we substitute the Fourier expansions $\Sigma_{\vec{\kappa}} \hat{f}_{\vec{\kappa}}(t) e^{i\vec{\kappa}\cdot\vec{x}}$ for each variable and express the resulting equations in terms of new scaled variables for the vertical vorticity $(\hat{\omega}_z)_{\vec{\kappa}}/\kappa_H$, the horizontal divergence (here written in terms of the vertical velocity) $-i\kappa\hat{w}_{\vec{\kappa}}/\kappa_H$, and the buoyancy $\hat{b}_{\vec{\kappa}} = g\hat{\rho}_{\vec{\kappa}}/\rho_o$. This procedure yields the following equations (Bartello 1995),

$$\frac{\partial \mathbf{W}_{\vec{\kappa}}}{\partial t} = i\mathfrak{L}(\mathbf{W}_{\vec{\kappa}}),$$

where

$$\mathbf{W}_{\vec{\kappa}} = \begin{pmatrix} \hat{\omega}_{z\vec{\kappa}}/\kappa_H \\ -i\kappa\ \hat{\omega}_{\vec{\kappa}}/\kappa_H \\ \hat{b}_{\vec{\kappa}}/N \end{pmatrix}$$

$$\mathfrak{L} = \begin{pmatrix} 0 & ifm/\kappa & 0 \\ -ifm/\kappa & 0 & -N\kappa_H/\kappa \\ 0 & -N\kappa_H/\kappa & 0 \end{pmatrix}.$$

Here $\vec{\kappa} = (k,l,m)$. With this choice of variables, the linear operator is Hermitian, and a complete set of orthogonal eigenvectors can be found. This ensures that a complete set of orthogonal eigenvectors can be found. The eigenvectors $\mathfrak{X}_{\vec{\kappa}}$ satisfy

$$\mathfrak{L}(\mathfrak{X}_{\vec{\kappa}}) = \sigma_{\vec{\kappa}}\mathfrak{X}_{\vec{\kappa}}.$$

Two of the eigenvalues,

$$\sigma_{\pm}(\kappa) = \pm\sqrt{\frac{N^2\kappa_H^2 + f^2m^2}{\kappa^2}}, \tag{7}$$

correspond to upward and downward propagating waves. Their associated eigenvectors are

$$\frac{1}{\sqrt{2}|\sigma_{\pm}|\kappa}\begin{pmatrix} \pm ifm \\ |\sigma_{\pm}|\kappa \\ \mp N\kappa_H \end{pmatrix}.$$

When $\vec{\kappa}_H = \vec{0}$, then $\hat{w}_z = 0$ from continuity, and the resulting wave eigenmodes have frequencies $\sigma_{\pm} = \pm f$.

The third root, $\sigma = 0$, with eigenvector

$$\frac{1}{\kappa|\sigma_{\pm}|}\begin{pmatrix} N\kappa_H \\ 0 \\ -ifm \end{pmatrix},$$

represents the nonpropagating (*PV*) mode. In this formulation, it is evident that the linear *PV* component of the flow field is horizontal and, when $f = 0$, it has no signature on the density field. Moreover, one can readily verify that only the mode with $\sigma = 0$ contributes to the potential vorticity.

The two flow invariants are energy and a truncated (quadratic) potential enstrophy. This truncation is necessary because the full enstrophy contains higher-order terms and is, therefore, not conserved by spectral spatial discretization. Further details on the truncation of potential enstrophy can be found in Warn (1986) or Bartello (1995).

3.3 Lagrangian Formulation

Rouhi & Abarbanel (1991) have used Lagrangian dynamics to derive a linear decomposition of strongly stratified flow into potential vorticity and wave components. They point out that the potential vorticity is exactly a quadratic function of the canonical variables in the Lagrangian formulation, whereas it is an infinite series in the velocity and density perturbations of the basic state in the Eulerian framework. They suggest, therefore, that solving the fully nonlinear interaction problem should be simpler in the Lagrangian framework. The details of this calculation have not, to our knowledge, been pursued.

3.4 Interactions Between the Wave and Potential Vorticity Components

We now examine in detail the types of interactions that can occur when both wave and *PV* components are taken into account. Most treatments of the interaction problem invoke some kind of multiple-scale formulation, based on the existence of two disparate time scales for the problem, namely $T_0 = 1/N$, characteristic of the rapid oscillations of the wave field, and an advective time scale $T_1 = L/U$ on which the *PV* component evolves. When the stratification is strong, the Froude number, defined as the ratio of T_0/T_1, becomes a small parameter, which we denote by μ, i.e.

$$F \equiv \frac{U}{NL} = \mu.$$

In the nonrotating case, with Equation 6, the velocity can be decomposed into wave and *PV* components, and the interaction problem can be formulated in terms of a set of three coupled nonlinear equations (derived from the full set of inviscid equations of motion) consisting of a wave equation, an evolution equation for potential vorticity, and an equation for the buoyancy ($b = -g\rho/\rho_0$) which is coupled to the wave equation through the buoyancy term. The crux of the multiple scale method is to treat the times $t_0 = t/T_0$ and $t_1 = t/T_1$ as independent variables. The time derivative is then written as

$$\frac{\partial}{\partial t} = \frac{\partial}{\partial t_0} + \mu \frac{\partial}{\partial t_1}.$$

We assume that the phase of the waves evolves on the fast time, whereas their complex amplitude is a function of the slow time. The *PV* component, on the other hand, is a function only of the slow time.

Note that, at the lowest order, potential vorticity and vertical vorticity are equivalent. The governing equations are then written:

$$\frac{\partial^2}{\partial t_0^2} \nabla^2 w + \nabla_h^2 w = -2\mu \frac{\partial^2}{\partial t_0 \partial t_1} \nabla^2 w + \mu(I_{ww} + I_{wv} + I_{vv}) \tag{8a}$$

$$\frac{\partial \nabla_h^2 \psi}{\partial t_0} = -\mu \frac{\partial}{\partial t_1} \nabla_h^2 \psi + \mu(J_{ww} + J_{wv} + J_{vv}) \tag{8b}$$

$$\frac{\partial b}{\partial t_0} + w = -\mu \frac{\partial b}{\partial t_1} + \mu(K_{ww} + K_{wv}) \tag{8c}$$

Here *I, J,* and *K* denote the nonlinear wave/wave, wave/*PV*, and *PV*/*PV* coupling terms. Equation 8b is, in fact, exactly the inviscid, nondiffusive form of the equation for potential vorticity, Equation 5. All flow variables are now expanded in power series of μ. For example, $w = w_0 + \mu w_1 + O(\mu^2)$. The uniform validity

of the solutions for sufficiently large times is ensured by imposing the constraint that each of the coefficients in the power series remains of $O(1)$ for all times (e.g. Kevorkian & Cole 1981). At the lowest order in μ, the equations are linear and decoupled. At the next order, contributions from the nonlinear interactions appear, along with the slow time dependence of the lowest-order solutions. Resonant conditions manifest themselves as secular terms in the right-hand sides of Equations 8a to 8c. The elimination of secularity yields slow-time evolution equations for the amplitudes of the lowest-order solutions, as is illustrated further in this section.

In the general case with rotation, the interaction problem can be formulated in terms of the coupled equations for conservation of energy and potential enstrophy. This is the approach taken by Warn (1986) in his study of nonlinear interactions between the wave and *PV* components in the shallow-water regime, and by Bartello (1995) in the present context. The resulting equations take the form

$$\frac{\partial}{\partial t_1}(E_k + E_p + E_q) = \sum_{\vec{\kappa}_k + \vec{\kappa}_p + \vec{\kappa}_q = \vec{0}} \text{nonlinear terms} = 0$$

$$\frac{\partial}{\partial t_1}(\sigma_k k^2 E_k + \sigma_p p^2 E_p + \sigma_q q^2 E_q) = \sum_{\vec{\kappa}_k + \vec{\kappa}_p + \vec{\kappa}_q = \vec{0}} \text{nonlinear terms} = 0,$$

where k, p, and q denote the wave numbers of the triad interaction components. Once again, the slow-time evolution of triad amplitudes is obtained by elimination of secular terms.

We also mention the approach of Babin et al (1997), using KAM (Kolmogorov–Arnol'd–Moser) theory. With this method, control of wave resonances is achieved via a mathematically sophisticated small-divisors analysis.

The important weakly nonlinear triad interactions between the wave and *PV* components are readily identified by considering initial states composed of at most a few modes.

3.4.1 Wave-Wave-Wave Resonant Triads We recall that two waves with phases $\vec{\kappa}_1 \cdot \vec{x} - \sigma_1 t$ and $\vec{\kappa}_2 \cdot \vec{x} - \sigma_2 t$ will resonantly force a third wave with wave vector $\vec{\kappa}_3$ if

$$\vec{\kappa}_3 = \vec{\kappa}_1 \pm \vec{\kappa}_2$$

and if the corresponding frequencies satisfy

$$\sigma_3 = \sigma_1 \pm \sigma_2,$$

where $\sigma_i = \sigma(\vec{\kappa}_i)$ as given by Equation 7. Resonant interaction theory was first derived by Phillips (1960, 1968) for surface and subsequently internal waves. The wave amplitude equations for the three waves are of the form

$$\frac{\partial \alpha_1}{\partial t_1} = \Gamma_{23}\alpha_2\alpha_3^*$$

$$\frac{\partial \alpha_2}{\partial t_1} = \Gamma_{31}\alpha_3\alpha_1^*$$

$$\frac{\partial \alpha_3}{\partial t_1} = \Gamma_{12}\alpha_1\alpha_2^*,$$

where the α_i are the amplitudes of the wave modes and the Γ_{ij} are the interaction coefficients (see, e.g. Lelong & Riley 1991). Triad interactions conserve both energy and a truncated (quadratic) version of potential enstrophy. Even though the interaction can produce some vertical vorticity, the potential vorticity remains zero (e.g. Lelong & Riley 1991). Therefore, no *PV* component can be excited from pure wave/wave interactions. Bartello's (1995) statistical mechanical arguments have shown that this class of resonances is of secondary importance in the evolution of rotating, stratified turbulence because energy exchanges are confined to the wave field for this weakly nonlinear case. Resonant internal wave interactions have been reviewed extensively (e.g. McComas & Bretherton 1977, Müller et al 1986, Phillips 1968).

One example in which resonant wave interactions might indirectly influence stratified turbulence is internal wave breakdown. It is well known (Drazin 1977, Klostermeyer 1984, Lombard & Riley 1996a, Mied 1976) that internal waves are unstable at any amplitude owing to a parametric subharmonic resonance. Numerical simulations (Bouruet-Aubertot et al 1995, Lin et al 1995, Lombard & Riley 1996b) have shown that this resonance mechanism can lead to fairly rapid growth of small-scale disturbances, resulting in a local breakdown of the wave into three-dimensional turbulence. Strong mixing can then occur, resulting in the generation of potential enstrophy and hence the appearance of stratified turbulence.

3.4.2 PV-PV-PV Triads The *PV-PV-PV* class of resonant triads is very broad because the resonance condition on the frequencies is trivially satisfied for any three *PV* modes with $\vec{\kappa}_1 \pm \vec{\kappa}_2 = \vec{\kappa}_3$. This is the only resonant triad present in two-dimensional turbulence, and it is also the dominant one in quasi-geostrophic (QG) turbulence, characterized by $Ro \ll 1$. It is responsible for the strong inverse energy cascades and downscale enstrophy cascade in two-dimensional and QG turbulence (Charney, 1971, Fjørtoft 1953). In the regime $Ro \geq 1$, the upscale transfer of energy is inhibited by an efficient downscale transfer of energy from *PV* to wave modes. This mechanism is discussed further below. Using an anisotropic EDQNM closure theory, Godeferd & Cambon (1994) have shown that triads of three vertical modes dominate in the initial stages of decay of stratified turbulence, and that they are responsible for the irreversible anisotropic structure created by stable stratification.

3.4.3 Wave-Wave-PV Triads The interaction of a wave $(\vec{\kappa}_1, \sigma_1)$ with a *PV* mode $(\vec{\kappa}_2, 0)$ will resonantly force a second wave of equal frequency σ_1 and wave vector $\vec{\kappa}_1 \pm \vec{\kappa}_2$. From Figure 2, it is clear that this class of resonances is quite broad because resonant triads involving waves of various wavelengths are allowed. In this resonance, conservation of potential vorticity implies that there can be no exchange of energy between wave and *PV* components. Therefore, the *PV* mode acts as a catalyst for the exchange of energy between the two waves (Bartello 1995, Babin et al 1997, Majda & Embid 1998, Embid & Majda 1996, Warn 1986, Lelong & Riley 1991). Catalytic behavior is also observed in the resonant interaction of a slowly varying horizontal shear and two equal-frequency internal waves with opposite inclination to the vertical. This mechanism, called elastic scattering, is believed to equalize upward and downward propagating internal-wave energy in the ocean (Phillips 1968). Milewski & Benney (1995) also note the presence of a catalytic interaction involving surface gravity waves and *PV* modes. In the present wave-wave-*PV* triad, there are no restrictions on the direction of vertical propagation of the waves, nor are the waves confined to the same vertical plane. In fact, Lelong & Riley showed that the interaction coefficients vanish if the two waves lie in the same vertical plane, and they postulated that this class of resonances would tend to isotropize the wave field in stratified turbulence. Bartello has demonstrated that this statement is consistent with statistical equilibrium arguments that predict that the energy must flow preferentially from large to small scales.

3.4.4 Wave-PV-PV Triads The only triad interaction that has the potential of directly initiating energy exchange between wave and *PV* modes involves two *PV* modes and one low-frequency wave. This interaction can never be exactly resonant but it can, nonetheless, be important, especially in stratified, nonrotating

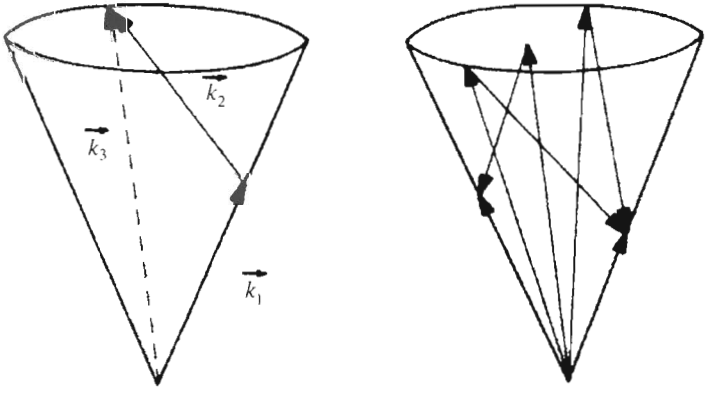

Figure 2 Examples of wave-wave-potential-vorticity triads (from Lelong & Riley 1991).

turbulence when $\kappa_1 \ll \kappa_2 \approx \kappa_3$ and $\omega_3 \approx 0$ (subscript 3 denotes the wave component). Bartello (1995) recognized the importance of this near-resonant triad in transferring *PV* mode energy to waves, where it can then be cascaded to small dissipative scales. When $f \neq 0$, wave frequencies cannot approach 0; therefore, the potential for significant energy transfer from the *PV* to the wave component is the greatest in stratified, nonrotating turbulence. In this regime, the wave-*PV*-*PV* interaction acts to drain energy away from the *PV*-*PV*-*PV* interaction. This may explain the absence of strong inverse energy cascades in strongly stratified, nonrotating flows.

Dong & Yeh (1988) have also studied nonresonant wave-*PV*-*PV* mode interactions. In contrast to the off-resonant triad discussed in the preceding paragraph, Dong & Yeh's triad is more likely to occur when $f \neq 0$. Their analysis, however, does not distinguish between potential and vertical vorticities. Therefore, their results remain ambiguous.

3.4.5 Dissipative Effects The mathematical analysis presented so far has been restricted to the inviscid regime. Embid & Majda (1998) have examined the effect of the Schmidt number *Sc* on the dissipation of stratified, rotating turbulence. For the regime of small *F* and finite *Ro*, they show that the diffusion coefficient for the wave field behaves as

$$-R_L^{-1}\frac{\kappa^2}{2}(1 + Sc^{-1}),$$

whereas that of the *PV* component is

$$-R_L^{-1}\kappa^2\left(\frac{\kappa_H^2 + F^2Sc^{-1}m^2}{\kappa_H^2 + F^2m^2}\right).$$

This result implies that, for large *Sc*, the wave motions decay at nearly one-half the rate of the slow *PV* modes at a given wave number. This result signals that caution should be used when comparing laboratory data with numerically simulated results, the latter of which normally imply $Sc \approx 1$.

3.5 Stability and Adjustment of Vortices

Smyth & McWilliams (1998) examined the effects of background stratification and rotation on the linear, inviscid stability of an axisymmetric columnar vortex. In particular, they focused on the transition between the nonstratified, nonrotating instability regime, which exhibits ultraviolet catastrophe (UVC), with no scale selection and monotonically increasing growth rates as the vertical wave number approaches infinity, and the quasi-gesotrophic regime with well-defined, fastest growing modal instabilities. Stratification is generally found to have a damping effect on the instability growth rate, though UVC behavior persists even as $F \rightarrow 0$. The presence of a weak rotation, on the other hand, tends to damp out UVC. This tendency is noted for Rossby numbers well beyond the $Ro \ll 1$ constraint

of quasi-geostrophy. In some instances, the instability results in the emission of a radiating inertia-gravity wave field.

Inertia-gravity waves are also generated during the adjustment of an unequilibriated, vertically confined vortex in a stratified, rotating environment. As the vortex strives to equilibriate, it will transfer some of its energy to a radiating wave field. In the strongly stratified, nonrotating regime, the final state is in cyclostrophic equilibrium and involves a horizontal balance between nonlinear inertial forces and the pressure gradient. (This is seen, for example, in some of the laboratory experiments discussed in Section 4.) The generated waves exhibit frequencies that are close to the buoyancy frequency, and the dominant wavelength scales as the radius of the adjusting vortex. The amount of wave energy E_{iw} released during adjustment is a function of the initial deviation from equilibrium. For strongly stratified conditions, E_{iw} is at most $O(F^2)$ (Lelong 1989, Lelong & McWilliams 1999). Moreover, the adjustment is insensitive to the sign of the vortex circulation because only the square of the azimuthal velocity enters into the final balance. When rotation is added, the final equilibrium includes the additional Coriolis force. The corresponding adjustment process, called gradient-wind adjustment to reflect the final gradient-wind balance (e.g. McWilliams 1988), results in a radiating inertia-gravity wave field with frequencies between the Coriolis and buoyancy frequencies. The Coriolis term removes the symmetry in the behavior of cyclonic and anticyclonic vortices. For a given pressure deviation from equilibrium, the amount of radiated wave energy remains $O(F^2)$ for anticyclones, but becomes $O(1)$ for cyclones. Bartello (1995) has shown that the wave-wave-PV triads are responsible for cascading wave energy downscale in nonlinear geostrophic adjustment.

4. LABORATORY EXPERIMENTS

Since the review of Lin & Pao (1979), a number of laboratory experiments have been conducted to better understand the dynamics of turbulence in stably stratified and sometimes rotating fluids. Some of these experiments have addressed the early stages of the flow development, including, for example, the radiation of internal waves from a turbulent region (Gilreath & Brandt 1985, Hopfinger et al 1991), the suppression of the vertical buoyancy flux and related dynamics (e.g. Lang 1982, Yap & van Alta 1993, Park et al 1994, Lin et al 1992, Itsweire et al 1986, Stillinger et al 1983), spectra and spectral energy transfer (Itsweire & Helland 1989), and the effects of current shear (Rohr et al 1988). Experiments addressing turbulent mixing were reported in the more recent review by Fernando (1991). A number of these experiments, however, either directly or indirectly addressed the later stages of decay of the turbulent region, i.e. the low Froude number regime. These include studies of wakes (both the wake of a sphere and the wake of a grid), horizontal jets (both pulsed and continuous), vertically ori-

ented grids oscillating in a direction normal to their plane, and specialized methods such as tangential injection.

In this section, we emphasize the low Froude number, PV component regime of these experiments, explaining both the origins of these motions and the relevant flow dynamics. We will see that, once the effects of stratification have begun to dominate the flow (i.e. the local Froude number has become small enough), the dynamics of the flow change in a dramatic and qualitatively similar manner in each case. Furthermore the subsequent flow development is representable by the scaling arguments presented in Section 2.

4.1 Wakes in Stably Stratified Fluids

By far the majority of the experiments addressing the low Froude number regime have dealt with the wake of a sphere moving horizontally through a stably stratified fluid. All of these experiments have utilized a towing tank configuration, as it is not possible to reach the late times necessary to obtain this regime in a wind tunnel or a water channel.

In the wake of a sphere moving through a stratified fluid, a number of physical processes occur that depend on the Froude and Reynolds numbers of the flow. The sphere itself generates an internal wave train that is approximately steady in the reference frame moving with the sphere. If the Reynolds number is high enough, the flow around the sphere separates into a turbulent wake in the lee of the sphere. The wake initially grows in the vertical and horizontal directions; the vertical growth is halted within a fraction of a buoyancy period, however, as the buoyancy forces limit the vertical motion of the fluid particles. (Here the buoyancy period is defined as $T_b = 2\pi/N$.) The turbulent wake decays as it radiates energy away in the form of internal waves and as it dissipates energy into heat. This wave radiation probably decreases the vertical component of the velocity relative to the horizontal components, helping to create a quasihorizontal motion. At some point the buoyancy forces begin to dominate the flow; that is, the local Froude number becomes small, and the character of the motion dramatically changes as described in the introduction for the experiments of Lin & Pao (1979).

These changes in the flow dynamics occur within several buoyancy periods. For example, Spedding et al (1996a,b) report that the wake is quasi-two-dimensional, in that the vertical velocity component is small compared with the horizontal component, beyond about $Nt = 2\pi t/T_b = 20$, or about three buoyancy periods. The local Froude number at this time is $F \sim 0.25$. Similar values for the critical Nt and F reported by Lin & Pao (1979) were 25 and 0.04, respectively.

Various experimental techniques are available to make detailed measurements of the velocity and density fields in the low Froude number regime and to infer, for example, the vorticity field. For example Fincham et al (1996) and Spedding et al (1996a,b) employed a customized digital particle image velocity technique to measure the horizontal velocity field on an isopycnal (constant density) surface. In a water tank linearly stratified with dissolved salt, neutrally buoyant polysty-

rene beads were placed in a preselected horizontal plane; for example, for wake experiments, the particles were generally placed in the midplane of the sphere. The sphere was towed horizontally through the tank, the motion of the beads was observed and recorded from CCD cameras placed above the tank, and the horizontal velocity field was inferred from the camera images. In the late wake, with little vertical displacement of the isopycnals (constant density surfaces), these isopycnals could be interpreted as constant z-surfaces. Then, in particular, the vertical vorticity ω_z and horizontal divergence Δ_z could be computed from these fields. Using the decomposition explained in Section 2, this allowed the total velocity field $\vec{u}$ to be decomposed into its internal wave component $\vec{u}_{iw}$ and *PV* component $\vec{u}_{pv}$ as

$$\omega_z = (\nabla \times \vec{u}_{pv})_z = \nabla_H^2 \psi$$

$$\Delta_z = \nabla_H \cdot \vec{u}_{iw} = \nabla_H^2 \phi.$$

Here ψ is a stream function defining the *PV* component of the field, and ϕ is a velocity potential defining the internal-wave component. As an alternative method, a technique was developed by Chomaz et al (1993b) that used horizontal fluorescene dye lines placed in the water before the run; they then observed the lines in the field of a laser light sheet. Density measurements were generally made with conductivity probes. Flow visualization of the wake was accomplished by using dye and observing it either with flood lighting or by laser-induced fluorescence (Gad-el-Hak et al 1981).

In the late wake, the vertical structure appears to be controlled by the Froude and Reynolds numbers. By carefully observing the separation lines of the wake at the surface of the sphere and using ideas for the separated vortices similar to those of Pao & Kao (1977), Chomaz et al (1992) have classified the different behavior of the wake as functions of the Froude and Reynolds numbers. Most specifically, for Froude numbers based on the speed and diameter of the sphere ($F_d = U/Nd$, where U and d are the speed and diameter of the sphere, respectively) less than about 4.5, the late wake motion is single-layered in the vertical; for $F_d \geq 4.5$, the wake is multilayered. [More recently, M Bonnier (private communication) suggests that the wake remains single-layered for much larger values of F_d than reported by Chomaz et al 1993a.] The rationale for the appearance of multiple layers is argued by Chomaz et al (1993a) and Spedding et al (1996a). If the overturning scale is greater than the scale of the turbulence, then multiple overturns are expected. Substituting in the experimental values of $u'/U \sim 0.3$ and $L/d \sim 0.4$ into the expression for F in the near wake leads to the condition

$$F_d \geq 3$$

for multiple overturns to occur, generally consistent with the observations.

The horizontal structure of the wakes appears to consist of quasi-two-dimensional, countersigned vortices, much like a two-dimensional wake, but with

vertical structure (Figure 3). Several authors remark as to how the flow in each horizontal plane is similar to two-dimensional flow. For example, Chomaz et al (1993a) point out the similarity of their flow to the two-dimensional numerical simulations of Couder & Basdevant (1986). The vortices tend to interact dynamically, sometimes pairing and sometimes forming dipoles. In the later stages of decay of the wake, however, the wake appears to consist mainly of weakly interacting monopoles.

Several authors have made detailed measurements of the velocity, density, and vorticity fields in individual monopoles. Interestingly, at least for the low Reynolds numbers characteristic of these experiments, the form of the monopoles is the same, independent of the initial state. For example, Bonnier et al (1998) performed experiments in the single-layer regime. Following Flór & van Heijst (1996), they assume an axisymmetric vortex, with the only nonzero component the azimuthal velocity, given by

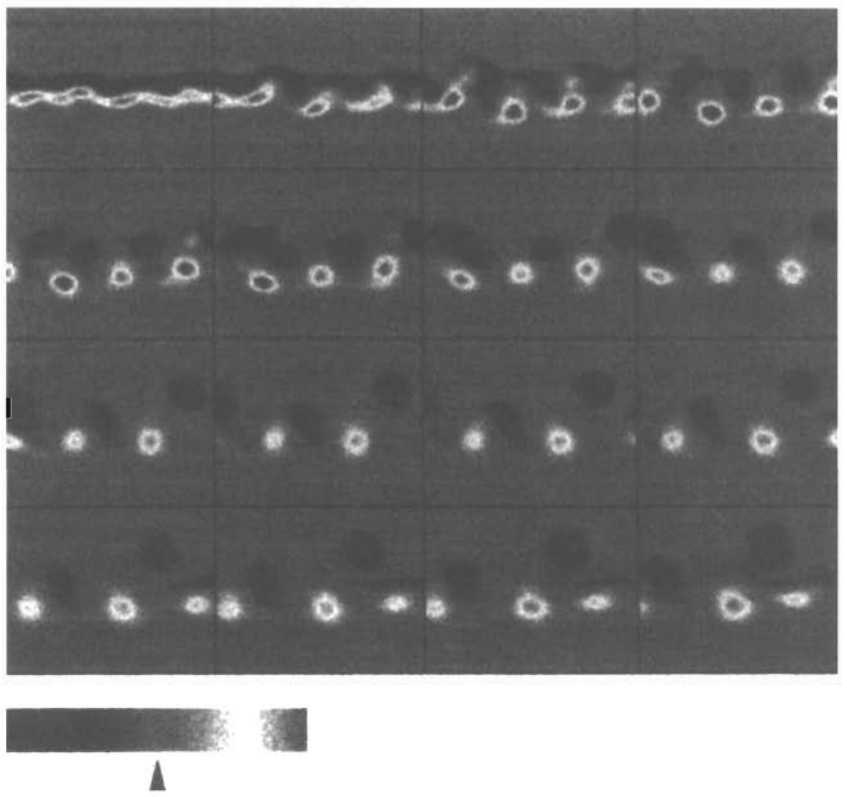

Figure 3 The vertical vorticity ω_z for 16 time steps spaced evenly in logarithmic time between $Nt = 21$ and $Nt = 640$; $R_d = 5286$; $F_d = 4$ (Spedding et al 1996a).

$$u_\theta = \frac{r}{r_m} V_r \exp\left[\frac{1}{2}\left(1 - \frac{r^2}{r_m^2} - \frac{z^2}{z_m^2}\right)\right].$$

Using the inviscid form of Equations 3a to 3d, they determined the fluctuating density and pressure fields as

$$p' = -\frac{\rho V_r^2}{2} \exp\left[\frac{1}{2}\left(1 - \frac{r^2}{r_m^2} - \frac{z^2}{z_m^2}\right)\right]$$

$$\rho' = -\frac{\rho V_r^2}{g} \frac{z}{z_m^2} \exp\left[\frac{1}{2}\left(1 - \frac{r^2}{r_m^2} - \frac{z^2}{z_m^2}\right)\right].$$

The physical picture is that the azimuthal velocity u_θ creates a centrifugal force that is balanced by the radial pressure gradient, i.e. the flow is in cyclostrophic balance. This pressure gradient varies in the vertical, however, inducing density fluctuations and causing the constant density surfaces to pinch toward the middle of the vortex. Such a model has previously been used in the low-Froude-number regime by Lelong (1989) and Lelong & McWilliams (1999) to explore the problem of vortex adjustment in a stratified fluid, as discussed in Section 3.6. Laboratory measurements (Bonnier et al 1998, Spedding et al 1996b, Trieling & van Heijst 1998) confirm this general picture.

Beckers et al (1998) have used the tangential injection method of Flór & van Heijst (1996) to generate isolated monopoles at very low Froude numbers. They also developed analytical solutions, based on experimental data, by using the viscous and diffusion forms of Equations 3a and 3d. The forms of the solutions are similar to those assumed by Bonnier et al. Again the results compare well with experiments, including the vertical diffusion and temporal decay of the flow.

Fincham et al (1996), in conducting experiments in the wake of an array of vertical rods, have combined the vertical structure and horizontal vortex structure of the wakes into one picture, which also appears to describe the wakes of spheres for $F_d \geq 4.5$ (see Figure 4). In a single horizontal plane, vortex lines are connected by a chain of vortex loops (Figure 4a), a stratified flow version of a Kármán vortex street. When other layers are present (Figure 4b), the layers are not decoupled, but are staggered, as shown in the figure.

The local Froude number at the time of collapse can be estimated from a straightforward scaling analysis. Assuming the the Froude number in the near field of the wake is large enough that the initial turbulence decay is not strongly affected by stratification, then, with $\varepsilon \sim u'^3/L$,

$$F = \frac{u'}{NL} \sim \frac{\varepsilon}{Nu'^2}.$$

Riley et al (1981) pointed out that, if u'^2 decays as t^{-n}, then ε should decay as t^{-n-1}. Therefore,

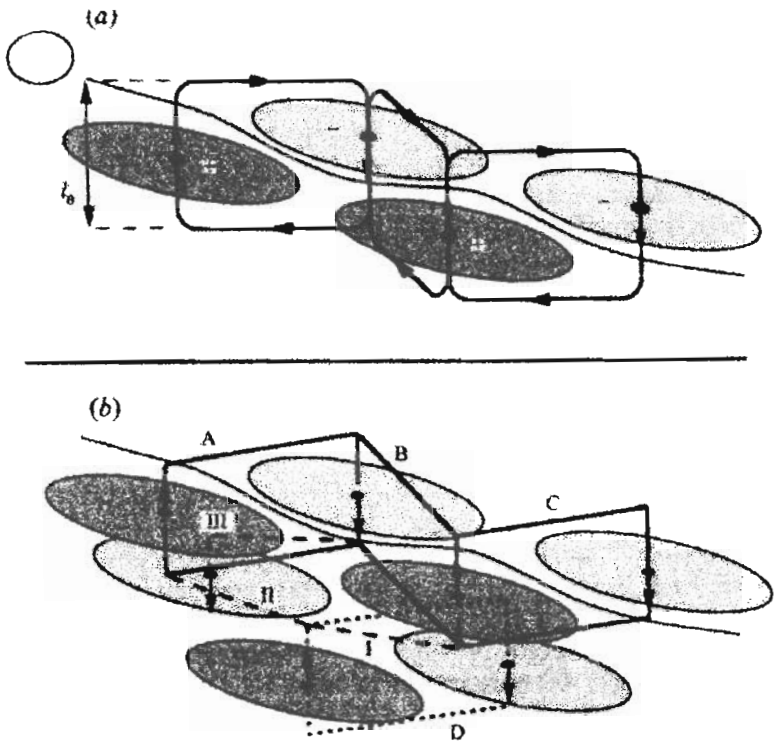

Figure 4 (a) Vortex lines loop between opposite-signed partners in a stratified version of the classical Kármán wake; (b) vortex loops of part (a) with a second layer added (Spedding et al. 1996b)

$$F \sim \frac{\varepsilon}{Nu'^2} \sim (Nt)^{-1}.$$

This implies that, assuming the initial Froude number is large enough, the local Froude number in the wake should be of order 1 within the decay time of a buoyancy period, independent of the initial Froude number.

Spedding et al (1996a,b) found that this relationship holds in both near and far wakes. Defining the Froude number in terms of the characteristic horizontal scale L_H, they found that

$$F \sim \mathcal{A}(Nt)^{-1}, \quad \mathcal{A} \sim 0.5.$$

At three-dimensional turbulence collapse ($Nt \sim 20$), then $F \sim 0.025$, in the same range as the values of Lin & Pao (1979). Similarly, Spedding et al found that the Reynolds number decays as

$$Re \sim \mathcal{B}(Nt)^{-1/3}, \ \mathcal{B} \sim 2.8 \cdot 10^3.$$

So, for example, at three-dimensional collapse, $Re \sim 1000$, already a rather low value, indicating that the flow is viscously dominated.

The vortices in the late wake appear to have a somewhat low aspect ratio α, thus providing the term "pancake eddies." For example, Bonnier et al (1998) measure $\alpha \sim 0.4$; Fincham et al (1996) find, for grid turbulence, $\alpha \sim 0.3$; whereas for vortex dipoles (see below), Voropayev et al (1995) find $\alpha \sim 0.4$, and Flór et al (1995) find $\alpha \sim 0.2$. This low aspect ratio is also consistent with the results of Fincham et al (1996) for the kinetic energy dissipation rate in the late wake of a grid. These authors directly measure the various terms defining the dissipation rate and find that it is dominated by the components giving the vertical shearing of the horizontal velocity. Assuming horizontal isotropy, they conclude that

$$\frac{dE}{dt} = -\varepsilon \simeq -2\nu\overline{\left(\frac{\partial u_1}{\partial z}\right)^2},$$

where E is the total kinetic energy. Fincham et al (1996) find that this component accounts for over 80% of the total kinetic energy dissipation rate, whereas the components with horizontal derivatives contribute very little. This implies that the vertical gradients are much larger than the horizontal gradients, and that the vertical scales are much smaller than the horizontal ones; that is, the vortices have low aspect ratio.

Majda & Grote (1997) and Majda et al (1999) have constructed exact laminar solutions for the low-Reynolds-number regime characteristic of the late stages of decay of the PV component by solving the evolution equations for this component. These solutions, which assume an initial state of periodic vortex dipoles embedded in a weak vertical shear, reproduce quite well the principal features of laboratory coherent structures. More specifically, the exact solutions exhibit a transition from nearly columnar vortices in a weakly vertically sheared mean flow to vertically layered pancake vortex sheets dominated by horizontal vorticity. This regime transition is accompanied by vigorous dissipation caused by the vertical shearing of the horizontal velocity.

Spedding et al (1996a,b) found that, in the late wake, the mean wake velocity deficit, measured in the centerplane of the wake, retains a self-similar, Gaussian form. Furthermore, surprisingly, the width of this profile grew as approximately $(x/d)^{1/3}$, and the peak velocity deficit decayed as $(x/d)^{-2/3}$, both the same rates as measured for nonstratified flows. The peak velocity, however, was much larger than its nonstratified counterpart. Furthermore, the centerline turbulence intensity decayed as $(x/d)^{-2/3}$, again the same rate as for the nonstratified case. It is not clear why these decay rates remain unchanged when the physical processes have changed so dramatically.

Finally, since a distinct Karman vortex street was observed in the far wake, the vortex spacing λ_x could be measured and a Strouhal number, $St = d/\lambda_x$,

determined. In the near field, Chomaz et al (1993b) and Bonneton et al (1996) observed that $St \sim F_d^{-2/3}$ for $F_d \leq 3$, but they observed no systematic F_d (dependence for higher F_d. In the far field, Spedding et al (1996a,b) found that $St \sim (Nt)^{-1/3}$, consistent with the $(x/d)^{1/3}$ growth rate of the wake, as monopole vortices continued to pair and merge.

4.2 Oscillating Vertical Grid

Another flow configuration used to examine turbulence in a stratified fluid is a turbulent front created by the oscillation of a vertical grid in the direction normal to the plane of the grid (e.g. Browand et al 1987, Ivey & Corcos 1982, Thorpe 1982). If both the Reynolds number ($S\omega M/\nu$) and Froude number ($S\omega/NM$) are sufficiently large, then the turbulent flow near the grid is approximately Reynolds number independent and behaves as if it were nonstratified. Here S, ω, and M are the stroke, frequency, and mesh spacing of the grid, respectively. Measurements in the nonstratified case (Hopfinger & Toly 1976) indicate that the turbulence decays away from the grid as

$$\frac{u'}{S\omega} \sim \mathcal{A}\,\frac{(SM)^{1/2}}{x},$$

the integral length scale grows as

$$\frac{L}{M} \sim \mathcal{B}\,\frac{x}{M}.$$

Here $\mathcal{A}$ and $\mathcal{B}$ are empirical constants. The local Froude number thus falls off as

$$F = \frac{u'}{NL} \sim \frac{\mathcal{A}}{\mathcal{B}}\left(\frac{\omega}{N}\right)\frac{(S^3M)^{1/2}}{x^2}. \tag{9}$$

At some distance from the grid, because of the increasing importance of the influence of buoyancy away from the grid, the three-dimensional motion collapses into quasihorizontal layers (see Figure 5). As the flow continues to develop, these layers propagate away from the grid in a manner similar to an intrusive front. The critical Froude number at which the collapse is measured to occur is $F_c \sim 0.25$ (Browand et al 1987), a value similar to that found for the breakdown in the wake of a sphere. The vertical spacing of the intrusions is given approximately by the value of L at collapse. From Equation 9, the distance to collapse is

$$\frac{x_c}{M} = \left(\frac{\mathcal{A}}{\mathcal{B}F_c}\right)^{1/2}\left(\frac{\omega}{N}\right)^{1/2}\left(\frac{S}{M}\right)^{3/4},$$

so that the vertical spacing is approximately

Figure 5 Turbulence collapse and intrusion formation; $\omega/N \approx 72$, $Nt = 25.4$ (Browand et al 1987).

$$\frac{L_c}{M} = \left(\frac{\mathcal{AB}}{F_c}\right)^{1/2} \left(\frac{\omega}{N}\right)^{1/2} \left(\frac{S}{M}\right)^{3/4} = \left(\frac{\mathcal{AB}}{F_c}\right)^{1/2} F_M^{1/2} \left(\frac{S}{M}\right)^{1/4}.$$

Here $F_M = U/NM$ is a Froude number based on the grid mesh spacing. In particular, the spacing decreases as the grid Froude number decreases as $L_c/M \sim F_M^{1/2}$.

4.3 Jets in Stably Stratified Fluids

The final experimental approach discussed here to investigate stratified flows is that of jets, both pulsed (e.g. Flór & van Heijst 1994, Flór et al 1995, van Heijst & Flór 1989) and continuous (e.g. Voropayev et al 1991, 1997). For example, in

the experiments of van Heijst and Flór, a small, pulsed round jet of fluid is injected horizontally into a tank of water linearly stratified with dissolved salt. The injected fluid has a density that is chosen to exactly match the density of the ambient fluid in the plane of injection. Typical Reynolds numbers based on the injection velocity U and nozzle diameter d ranged between 360 and 11,500. The Froude number at the jet exit tended to be very large, and the flow initially developed unaffected by buoyancy. An isolated turbulent region forms, but on the order of a buoyancy period collapsed into a thin, pancake-shaped region, with quasihorizontal flow. Internal waves were generated by this process, but they propagated away from the pancake-eddy region and did not appear to directly affect the subsequent flow development. In this regime horizontally oriented eddies interact and merge and, ultimately, a dipolar structure is formed (see Figure 6). The structures tended to be single layered in the vertical, due to the method of injection of fluid of single, matched density.

In the collapsed region the Reynolds and Froude numbers are very low. Typically, $Re \sim 100$ and $F \sim 0.1$, so that the flow is both viscously and buoyantly dominated. The velocity in the dipole structure was observed to decay mainly because of vertical diffusion and the horizontal entrainment of irrotational fluid (Flór & van Heijst 1994). In order to describe this flow, Flór et al (1995) started

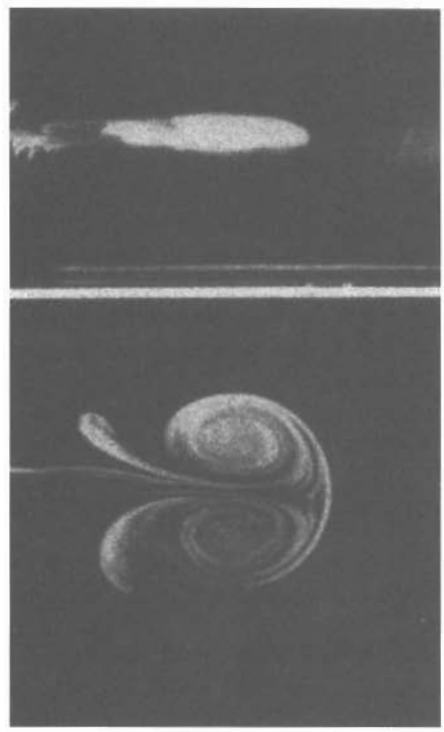

Figure 6 Photograph showing the top view and side view (*lower* and *upper* parts of the figure, respectively) of dye-visualized dipolar flow (Flór et al 1995).

with the scaling analysis for the *PV* component discussed in Section 2, writing the equations in terms of the vertical vorticity ω_z and the stream function of the horizontal motion ψ. To solve these equations, the Lamb-Chaplygin dipole model (Lamb 1932) was employed, which assumes a linear relation between ω_z and ψ and that $\omega_z = 0$ in the flow exterior to the dipole, $r > a$, where a is the dipole radius.

To deal with the horizontal entrainment of the dipole and with its vertical structure and vertical diffusion, Flór et al (1995) considered two different models. In the first model the dipole (vertical) thickness and radius were assumed constant, whereas in the second the increasing vertical thickness of the dipole was taken into account. In both cases the predictions of the models agree fairly well with the laboratory data, for example, with the decay rates of the horizontal velocity and vertical vorticity. Interestingly, the dipole vortices appeared to decay exponentially in time, whereas the monopole vortices (Spedding et al 1996a,b) exhibited power law decay.

Voropayev et al (1997) carried out experiments with a continuous jet introduced into a rotating, stably stratified fluid. Again the three-dimensional flow collapses away from the nozzle, becoming quasihorizontal. Interestingly, the shape of the leading edge of the continuous jet depends on the ratio N/f. When the rotation rate is somewhat strong compared with the stratification (i.e. the Coriolis forces are able to significantly modify the flow in a buoyancy period), e.g. for $N/f \leq 10$, the jet deflects to the right of the x-axis. (The tank is rotated in the counterclockwise direction about the z-axis.) A spiral monopole is formed in a relatively thin horizontal layer. As the rotation rate is decreased, buoyancy forces come in more quickly relative to the Coriolis forces. For $N/f > 10$, the leading edge takes the form of a dipole, as in the nonrotating case. The authors present a theoretical model that predicts, in particular, the transition between the two regimes.

5. NUMERICAL SIMULATIONS

A number of numerical simulations have been carried out to address various issues related to turbulence in stably stratified fluids. These include studies of homogeneous decay (e.g. Gerz & Yamazaki 1993, Métais & Herring 1989, Ramsden & Holloway 1992, Riley et al 1981), homogeneous shear flows (e.g. Galmiche unpublished results 1998; Gerz et al 1989, Holt et al 1992, Jacobitz et al 1997), turbulent free shear layers (e.g. Staquet 1995, Staquet & Riley 1989a), stable atmospheric boundary layers (e.g. Barnard 1999, Mason & Derbyshire 1990), and the breakdown of internal waves (e.g. Andreassen et al 1998, Bouruet-Aubertot et al 1995, Fritts et al 1998, Lelong & Dunkerton 1998a,b, Lin et al 1995, Lombard & Riley 1996b, Winters & D'Asaro 1994). A number of issues have been addressed in these simulations, including explanations of the development of countergradient fluxes, the character of large-scale structures, critical Richardson

numbers in shear flow turbulence, turbulence energetics (including both kinetic and potential energies), and spectral-energy transfer. As in the previous section on laboratory studies, we focus on numerical simulations that shed light on the dynamics of the *PV* component, that is, the low-Froude-number regime.

Various numerical methods have been used in simulating turbulence in stably stratified fluids, although in many studies statistical homogeneity has been assumed and Fourier-spectral methods employed (Canuto et al 1988). In the studies discussed in this section, spectral (or pseudo-spectral) methods have been utilized.

Numerical simulations have proven to be a useful tool in the study of turbulence in stratified fluids. From the complete snapshot of the flow provided at every time step, many statistical quantities can be computed that cannot be measured in the laboratory; in addition, the flow field can be visualized in various ways. Hence, numerical simulations have often been instrumental in helping interpret laboratory data and have also contributed much to the understanding of theoretical issues such as the energy cascade in stratified turbulence.

The principal drawback of numerical methods remains the relatively low spatial resolution attainable, limiting the range of spatial and temporal scales that can be realistically simulated. Hence, the maximum Reynolds numbers of numerically simulated flows are still well below typical values encountered in geophysical flows. For example, three-dimensional direct numerical simulations with a computer code employing pseudospectral numerical methods and a resolution of 128^3 collocation points yield values of only $Re_\lambda \approx 80$ (Kimura & Herring 1996), where Re_λ is a Reynolds number based on the Taylor microscale. Typical values of Re_λ in the atmosphere can extend into the thousands or more.

To partially alleviate the limitations brought about by modest resolution, some numerical studies have utilized large-eddy simulation techniques to maximize the range of simulated energetic scales. (See Lesieur & Métais 1996 in this same series for a recent review of large-eddy simulations.) One commonly used LES method employs a hyperviscous operator ∇^n (where $n \geq 4$) to parameterize viscous damping in place of the Laplacian molecular diffusion operator. Hyperviscosity effectively restricts the influence of viscous dissipation to a very narrow range (which decreases as n is increased) near the cutoff wave number. Hyperviscosity undoubtedly owes its popularity to the fact that it is trivially implemented in pseudospectral codes, since powers of the Laplacian are simply expressed as powers of κ^2 in spectral space. The use of hyperviscosity is justified by studies such as that of Borue & Orszag (1996) for three-dimensional, decaying turbulence, which have demonstrated the insensitivity of the large, energy-containing scales to the form of the dissipation parameterization used. More elaborate dissipation parameterizations such as Smagorinsky's (Kaltenbach et al 1994, Siegel & Domaradzki 1994), structure-function subgrid-scale models (Métais & Lesieur 1992), and Richardson-number-dependent formulations have also been used with similar success, although they are not as easily implemented as hyperviscosity. The current rapid development of parallel computing (e.g. de Bryun

Kops & Riley 1998, Werne & Fritts 1999) appears promising and will bring turbulence simulation to an unprecedented degree of realism in the coming decade.

The numerical simulations considered here fall into the two broad categories of decaying and forced turbulence.

5.1 Decaying Turbulence Under the Influence of Stratification

Several studies of decaying turbulence employing direct numerical simulations have been conducted that have addressed the low Froude number regime and the dynamics of the internal wave and *PV* components. For example, in addition to introducing the scaling arguments and flow decomposition discussed in Section 2, Riley et al (1981) presented results of simulations of homogeneous, decaying turbulence in density-stratified fluids. They found, in particular, that as the Froude number became small, the flow nonlinearity still remained large, although certain nonlinearities were inhibited, e.g. those related to the term $w\partial w/\partial z$ in the vertical component of the momentum equation (see Equation 2). This latter effect appeared to result in a slightly weakened energy dissipation rate. Riley et al also found that, compared to the decay of turbulence without density stratification, the growth of horizontal scales was enhanced, whereas that for vertical scales was inhibited. In addition, qualitatively consistent with the laboratory results presented in the previous section, the horizontal component of the vorticity became larger than the vertical component.

Métais & Herring (1989) performed a careful series of direct numerical simulations of homogeneous decay to address, in particular, the low Froude number regime, employing in their analysis the velocity field decomposition discussed in Section 2. Their numerical results generally agreed with the experimental data of Itsweire et al (1986) with respect to the major statistical descriptors, giving confidence in their methodology. Some differences were noted in the behavior of the buoyancy flux, as the simulation values were about a factor of 2 larger than the laboratory values. In the simulations, the Schmidt number is of order 1, whereas it is about 200 in the laboratory experiments of Itsweire et al, in which salt stratification in water is employed. Recently, laboratory experiments in temperature-stratified wind tunnels (Lienhard & van Atta 1990, Yoon & Warhaft 1990), in which the Schmidt (or, more correctly, the Prandtl) number is of order 1, show trends in the buoyancy flux similar to the results from the numerical experiments.

In the small Froude number regime, Métais & Herring (1989) found that their results were very sensitive to initial conditions, depending, for example, on the ratio of the internal wave energy to the stratified turbulence (*PV* component) energy. In simulations initialized with stratified turbulence but no internal waves, they found that very little internal wave energy was generated; they also found that more kinetic energy dissipation occurred than for strictly two-dimensional

turbulence and that the dissipation was caused by the vertical shearing of the horizontal velocity, again in qualitative agreement with the laboratory results presented in the previous section. They identified flow "collapse" in terms of a collapse of the Thorpe scale (Thorpe 1977) and found that this occurred at about $Nt \sim 6$ and $F \sim 0.25$, again qualitatively consistent with laboratory results. As with the results of Riley et al, Métais & Herring noted the tendency for enhanced growth of horizontal scales and inhibited growth of vertical scales.

Holt et al (1992) focused mainly on homogeneous, sheared turbulence at higher Froude numbers. Regarding the low-Froude-number regime, they did note that, at late times and for weaker shears, nonlinear spectral energy transfer was somewhat suppressed by the stable stratification, and the vertical velocity and density fields were approximately 90° out of phase, consistent with the existence of an internal-wave field.

Bartello (1995) performed some numerical simulations of decaying stratified turbulence. His close examination of the various energy transfer terms reveals that, in the regime with low F, $Ro = O(1)$, wave and PV motions are inherently coupled, with the predominant exchange mechanism being the off-resonant triad discussed in Section 3.4.4. This is in contrast to the low-F, low-Ro quasi-geostrophic regime in which the two types of motion evolve independently of each other.

In addition to turbulence dynamics, Kimura & Herring (1996) focused on fluid particle dispersion in turbulence in a stably stratified fluid; they found that both single-particle dispersion and particle pair separation were inhibited in the vertical direction by stable stratification, while being relatively unaffected in the horizontal. Moreover, the late stages of the flow exhibited regions of intense viscous dissipation characterized by large horizontal vorticity, consistent with the laboratory measurements of Fincham et al (1996).

Gerz & Yamazaki (1993) initialized their simulations with buoyancy perturbations to simulate the conditions of fossil turbulence. They analyzed the flow behavior in terms of a stratification number Sn, defined as the ratio of perturbation-to-background temperature gradients. They found that, when $Sn < 1$, the flow remained in a transient state of turbulence in which stirring and mixing were observed.

5.2 Forced Turbulence Under the Influence of Stratification

One of the conjectures that has motivated several numerical studies of stratified turbulence is whether the inverse cascade mechanism envisioned by Gage (1979) and Lilly (1983) to explain atmospheric mesoscale energy spectra is possible. To address this issue, a number of simulations have been performed, utilizing a variety of forcing mechanisms to simulate small-scale energy sources.

Herring & Métais (1989) devised a series of forced, nonrotating ($Ro = \infty$) calculations with increasing values of N. In all cases, a random Markovian forcing was applied to the horizontal velocity components over a narrow range of wave-

number magnitudes, $10 < \kappa < 12$, where the full range of wave number magnitudes is $1 < \kappa < 32$. A first calculation involved purely two-dimensional Markovian forcing and no vertical variability (i.e. vertical velocity and density perturbations were set to zero initially). As anticipated, the flow remained two-dimensional and developed a vigorous $\kappa_H^{-5/3}$ inverse cascade to the left of the forcing wave number k_f (Figure 7) in agreement with two-dimensional forced turbulence theory (Kraichnan 1967). When vertical variability, in the form of small three-dimensional density perturbations, was added to the initial conditions, the evolution of the flow changed dramatically. In particular, a comparison of the two most stratified cases ($N = 40\pi$, 80π) reveals little change in the behavior, consistent with the scaling analysis presented in Section 2 (Figure 7b). The kinetic energy of the wave component and the potential energy grew exponentially at a rate independent of the stratification until they became saturated. Moreover, the three-dimensional variability appeared to allow substantial energy transfer to smaller scales and hence to inhibit both the transfer of energy to large scales and the development of an inverse $\kappa_H^{-5/3}$ regime.

As the stratification was increased, the velocity field became more horizontal. It remained very much three-dimensional, however, in that frictional dissipation between adjacent horizontal layers continued to drain the energy of the stratified turbulence component. This interlayer drag acted on all horizontal scales and effectively flattened the slope of the energy spectrum at scales larger than the forcing scale. Hence, a $\kappa_H^{-5/3}$ spectrum was not observed. Examination of the various energy transfer terms confirms that the *PV*/*PV* mode interactions, responsible for the upscale transfer in the two-dimensional case, were then in competition with an efficient wave/*PV* mode interaction that cascaded *PV* component energy to smaller scales. Bartello (1995) demonstrated the role of this interaction,

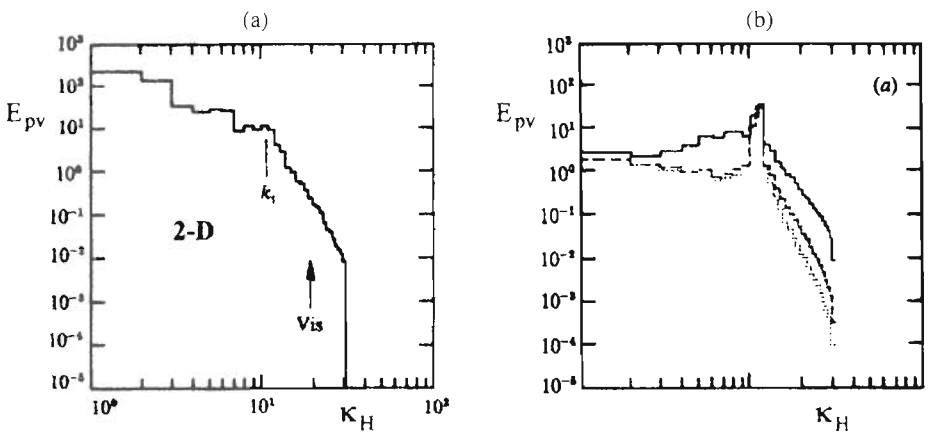

Figure 7 Horizontal energy spectra for (a) purely two-dimensional case and (b) three values of N; from Herring & Métais 1989.

composed of near-resonant slow-slow-fast triads (described in Section 3), in facilitating the transfer of energy from the stratified turbulence to the wave component. As pointed out earlier, this triad becomes less important when rotational effects are present.

Métais et al (1994) repeated the previous simulations of Herring & Méais (1989) with both two-dimensional and three-dimensional forcing and with various degrees of rotation. For the case with two-dimensional forcing, a small three-dimensional perturbation, and weak rotation ($N/f = 10$), more energy was transferred out of the forcing region to larger horizontal scales than in the analogous case without rotation. Only when $N/f = 1$ with $F \ll 1$, however, does a $\kappa_H^{-5/3}$ inverse cascade clearly emerge. This is the familiar geostrophic regime.

More recently, Vallis et al (1996) presented results of convectively driven turbulence at the atmospheric mesoscale obtained with a meteorological model featuring the inclusion of water vapor, bottom boundary layer effects, variable $N(z)$, and a Richardson-number-dependent subgrid-scale parameterization; they reported the existence of an inverse $\kappa_H^{-5/3}$ cascade in both rotating and nonrotating regimes. The model, however, had very limited vertical resolution. Similar results have been reported by Lilly et al (1998), again with very limited vertical resolution. In particular, the limited vertical resolution of these meteorological studies does not resolve the overturning scale L_o. Although there are many disparities between idealized stratified turbulence simulations (e.g. of Herring & Métais 1989) and these more realistic convective cloud and storm simulations, which undoubtedly have some effect on differences in the solutions, Bartello (1999) suggests that the different vertical resolutions, and hence the different vertical dissipation in the two types of studies, can account for the discrepancies in the behavior of the energy cascades. He argues that if the overturning scale is smaller than the model grid resolution, one should not expect overturning because it is not resolved. Therefore, individual isopycnal surfaces are rendered coherent, and the flow will behave more two-dimensionally.

To clarify this matter, Bartello (1999) has performed some simulations to investigate the sensitivity of the inverse cascade to vertical dissipation. To mimic the effect of different vertical resolutions, additional dissipation terms proportional to $\nu_z m^2$ are included in the momentum and buoyancy equations, where m is the vertical component of the wave number vector and ν_z is an artificial viscosity applied in the z-direction. The vertical dissipation is controlled by varying ν_z. As seen in Figure 8 (Bartello 1999), the largest value of ν_z results in a clear $\kappa_H^{-5/3}$ cascade. As ν_z is decreased, however, the $\kappa_H^{-5/3}$ spectrum disappears. Therefore, it appears that the strong inverse cascade is only possible if the vertical variability, and hence strong cascade to smaller scales, is inhibited.

5.3 Coherent Structures in Stratified Turbulence

An issue that is closely related to the presence of an inverse cascade is the existence of coherent structures in stratified turbulence. Coherent structures routinely develop in the late stages of numerically simulated, two-dimensional and quasi-

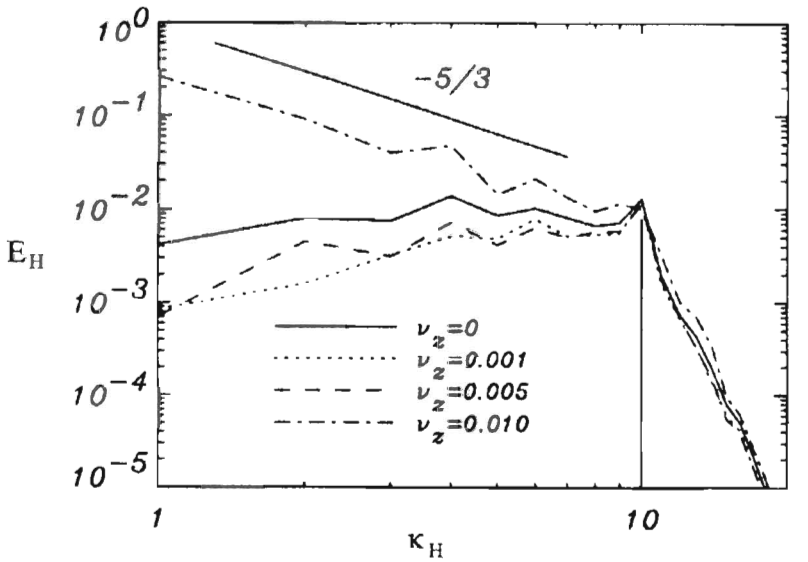

Figure 8 Horizontal energy spectra $E(\kappa_H)$ for forced simulations with $N/f = 100$ at various vertical dissipations (Bartello 1999). The *vertical line* indicates the forced wave number κ_f.

geostrophic turbulence (e.g. McWilliams 1990a,b, McWilliams et al 1994), as inverse cascade continually increases the scale of the flow field. As discussed in the previous section, meandering, quasi-two-dimensional structures are also commonly visualized in the late stages of laboratory experiments with stable stratification. Kimura & Herring (1996), using vertical vorticity to visualize the motions, obtained scattered, pancakelike structures. Winters & D'Asaro (1994), using potential vorticity as a tracer, found pancake structures in their three-dimensional simulations of wave breakdown at a shear-flow critical level. Unfortunately, in almost all of the other numerical simulations to date, there has been little attempt to simulate the visualization results from the laboratory, e.g. by simulating dye dispersion in the flow. Such simulations could help determine how closely the numerical simulations replicate the laboratory experiments.

6. FINAL COMMENTS

A number of issues related to the *PV* component remain unresolved, the most important of which are in regard to the dynamics. For example, how do the dynamics of stratified turbulence differ from those of two-dimensional turbulence, especially given the potential for vertical variability? Some of the laboratory and numerical experiments indicate that there are great similarities between the two.

The numerical experiments of Herring & Métais (1989) without rotation indicate, however, the tendency for small scales to develop in the vertical, as well as a weakening of upscale transfer of energy to larger scales in the horizontal as the vertical variations develop.

Related to this is the question of what determines the vertical scale of the motion. In the laboratory experiments and numerical simulations, the vertical scale appears to be controlled by the viscosity. In both cases, the Reynolds numbers tend to be low. Lilly (1983) argues that, for much higher Reynolds number flows representative of geophysical flows, adjacent horizontal layers will tend to decorrelate, resulting in shear instabilities and turbulence. Thus the vertical scale may be set by the properties of the turbulence. Voropayev et al (1997) have suggested that the laboratory experiments might scale up to geophysical scales as long as the viscosity in the laboratory experiments is replaced by a turbulent viscosity in the geophysical case.

Drawing conclusions similar to Lilly's, but using spectral energy transfer arguments, Bartello (1999) points out that high-Reynolds-number flows may favor a transfer of energy to smaller scales through instabilities and turbulence, resulting in a significantly less effective upscale transfer. This suggests that the results of laboratory experiments and numerical simulations may not apply at geophysical scales.

Recent laboratory experiments and stability analysis (Billant 1999; P Billant & JM Chomaz, unpublished observations) suggest the existence of a 'zigzag' instability in strongly stratified flows. The instability has a vertical scale L_V of order N/u', so that $F \sim 1$; its existence offers, in particular, a possible explanation of the rapid development of small vertical scales in the experiments of Herring & Métais (1989). The 'zig-zag' instability bears resemblance to the 'tall-column' instability of quasi-geostrophic vortices (Dritschel & de la Torre Juárez 1996). In the quasi-geostrophic regime, however, there is increased vertical coherence due to the strong effect of rotation. Recent numerical simulations of the evolution of columnar vortices in this regime (Dritschel et al 1999) confirms the inherent three-dimensionality of this flow. They find that three-dimensional dynamics dominate when the radius of the vortices is the same order as the Rossby radius of deformation.

Métais et al (1994) repeated the numerical experiments of Herring & Métais, but with rotation. In these preliminary simulations it was found, as expected, that with increasing rotation rate the development of vertical variability is reduced. This resulted in enhanced upscale energy transfer, more like two-dimensional turbulence or quasi-geostrophic turbulence. Therefore rotation clearly influences the overall dynamics.

Another aspect of the dynamics is how the stratified turbulent interacts with the internal-wave field. Interactions are expected to be weak because of the differences in time scales. As Lelong & Riley (1991), Bartello (1995), and Embid & Majda (1996) have pointed out, however, the *PV* component can strongly affect the spectral-energy transfer in the internal-wave field. In addition, it is expected that the *PV* component is a source of internal waves. As various *PV* component

features interact, vertical motions can be generated, and internal waves result. A theory is lacking, however, to predict the efficiency of the *PV* component as a source for internal waves. It is also possible for internal waves to be a source of the *PV* component, as internal waves break down into three-dimensional turbulence; this can cause strong mixing and the generation of potential enstrophy, and hence the *PV* component, as in the numerical simulations of Staquet & Riley (1989a), Winters & D'Asaro (1994), and Lombard & Riley (1996b). The properties of the *PV* component resulting from wave breakdown remain to be determined.

Finally, ambient conditions, for example, the vertical density structure and current shears, could have a profound effect of the generation, development, and decay of stratified turbulence. These effects also remain to be determined.

ACKNOWLEDGMENTS

We would like to thank P. Bartello, M. Bonnier, J. Flór and W. Smyth for valuable comments on an earlier version of the manuscript. G. Spedding, F. Browand, J. Flór, J. Herring and P. Bartello kindly provided figures. Both authors would especially like to thank J. Herring for many useful, enlightening discussions of geophysical turbulence. Support for M.-P. Lelong was provided by the NSF (grants OCE-9811939 and OCE-9521275).

LITERATURE CITED

Ahlnas K, Royer TC, George TM. 1987. Multiple dipole eddies in the Alaska Coastal Current detected with Landsat Thematic Mapper data. *J. Geophys. Res.* 92:13041

Andreassen O, Hvidsten PO, Fritts DC, Arendt S. 1998. Vorticity dynamics in a breaking internal gravity wave. Part 1. Initial instability evolution. *J. Fluid Mech.* 367:27–46

Babin A, Mahalov A, Nicolaenko B, Zhou Y. 1997 On the asymptotic regimes and the strongly stratified limit of rotating Boussinesq equations. *Theor. Comp. Fluid Dynam.* 9:223–51

Barnard JC. 1999. *A numerical study of the very stable Ekman layer.* PhD thesis. Univ. Wash. Seattle.

Bartello P. 1995. Geostrophic adjustment and inverse cascades in rotating stratified turbulence. *J. Atmos. Sci.* 52:4410–28

Bartello P. 1999. Potential vorticity, resonance and dissipation in rotating convective turbulence. *Geophys. Astrophys. Conv.* In press

Beckers M, Verzicco R, Clercx HJH, van Heijst GJF. 1998. The vertical structure of pancake-like vortices in a stratified fluid: experiments, theory and numerical simulations. *J. Fluid Mech.* Submitted

Billant P. 1999. *Dynamique d'une paire de tourbillons verticaux en milieu stratifié.* thèse, Docteur de L'École Polytechnique, Paris

Bonneton P, Chomaz JM, Hopfinger EJ, Perrier M. 1996. The structure of the turbulent wake and the random wave field generated by a moving sphere in a stratified fluid. *Dyn. Atmos. Oceans* 23:299–308

Bonnier M, Eiff O, Bonneton P. 1998. On the density structure of far-wake vortices in a stratified fluid. *Dyn. Atmos. Oceans.* In press

Borue V, Orszag SA. 1996. Self-similar decay of three-dimensional homogeneous turbulence with hyperviscosity. *Phys. Rev. E.* 51(2):856–59

Bouruet-Aubertot P, Sommeria J, Staquet C. 1995. Breaking of standing internal gravity waves through two-dimensional instabilities. *J. Fluid Mech.* 285:265–301

Briscoe MG. 1975. Preliminary results from the trimoored internal wave experiments (IWES). *J. Geophys. Res.* 80:3877–84

Browand FK, Guyomar D, Yoon SC. 1987. The behavior of a turbulent front in a stratified fluid: experiments with an oscillating grid. *J. Geophys. Res.* 92:5329–41

Bryan FD. 1986. *Maintenance and variability of the thermohaline circulation.* PhD thesis. Princeton Univ. 158 pp.

Bryan FD. 1987. Parameter sensitivity of primitive equation ocean general circulation models. *J. Phys. Oceanogr.* 17:970–85

Canuto C, Hussaini MY, Quarteroni A, Zang TA. 1988. *Spectral Methods in Fluid Dynamics.* New York: Springer

Charney JG. 1971. Geostrophic turbulence. *J. Atmos. Sci.* 28:1087–95

Chen L, Young WR. 1995. Density compensated thermocline gradients and diapycnal fluxes in the mixed layer. *J. Phys. Oceanogr.* 25:3064–75

Cho JYN, Newell RE, Barrick JD. 1999. Horizontal wave number spectra of winds, temperature, and trace gases during the Pacific Exploratory Missions: Z. Gravity waves, quasi-two-dimensional turbulence, and vortical modes. *J. Geophys. Res.* 104:16,297–16,308.

Chomaz JM, Bonneton P, Butet A, Perrier M, Hopfinger EJ. 1992. Froude number dependence of the flow separation line on a sphere towed in a stratified fluid. *Phys. Fluids* A4:254–58

Chomaz JM, Bonneton P, Butet A, Hopfinger EJ. 1993a. Vertical diffusion of the far wake of a sphere moving in a stratified fluid. *Phys. Fluids* A5(11):2799–806

Chomaz JM, Bonneton P, Hopfinger EJ. 1993b. The structure of the near wake of a sphere moving horizontally in a stratified fluid. *J. Fluid Mech.* 254:1–21

Couder Y, Basdevant C. 1986. Experimental and numerical study of vortex couples in two-dimensional flows. *J. Fluid Mech.* 173:225–51

Cummins PFG, Holloway G, Gargett AE. 1990. Sensitivity of the GFDL ocean general circulation model to a parameterization of vertical diffusion. *J. Phys. Oceanogr.* 20:817–30

de Bruyn Kops SM, Riley JJ. 1998. Direct numerical simulation of laboratory experiments in isotropic turbulence. *Phys. Fluids* 10:2125–27

Dong B, Yeh KC. 1988. Resonant and nonresonant wave-wave interactions in an isothermal atmosphere. *J. Geophys. Res.* 93:3729–44

Dougherty JP. 1961. The anisotropy of turbulence at the meteor level. *J. Atmos. Sol. Terr. Phys.* 21:210

Drazin PG. 1961. On the steady flow of a fluid of variable density past an obstacle. *Tellus* 13:239–51

Drazin PG. 1977. On the instability of an internal gravity wave. *Proc. R. Soc. Lond.* 356:411–32

Dritshcel DG, de la Torre Juárez M. 1996. The instability and breakdown of tall columnar vortices in a quasi-geostrophic fluid. *J. Fluid Mech.* 328:129–160

Dritschel DG, de la Torre Juárez M, Ambaum MHP. 1999. The three-dimensional vortical nature of atmospheric and oceanic turbulent flows. *Phys. Fluids* 11:1512–20

Embid PF, Majda AJ. 1996. Averaging over fast gravity waves for geophysical flows with arbitrary potential vorticity. *Commun. Partial Differ. Equ.* 21(3&4):619–58

Embid PF, Majda AJ. 1998. Low Froude number limiting dynamics for stably stratified flow with small or finite Rossby numbers. *Geophys. Astrophys. Fluid Dyn.* 87:1–50

Eriksen CC. 1978. Measurements and models of finestructure, internal gravity waves, and wave breaking in the deep ocean. *J. Geophys. Res.* 83:2989–3009

Ertel H. 1942. Ein neuer hydrodynamischer wirbelsatz. *Meteorol. Zeit.* 59:271

Etling D. 1989. On atmospheric vortex streets in the wake of large islands. *Meteorol. Atmos. Phys.* 41:157–64

Fedorov KN, Ginsburg AI. 1989. Mushroom-like currents (vortex dipoles): one of the most wide-spread forms of non-stationary coherent motions in the ocean. In *Mesoscale/Synoptic Coherent Structures in Geophysical Turbulence,* ed. JCJ Nihoul, pp. 15–24.

Fernando HJS. 1991. Turbulent mixing in stratified fluids. *Annu. Rev. Fluid Mech.* 23:455–93

Fincham AM, Maxworthy T, Spedding GR. 1996. Energy dissipation and vortex structure in freely-decaying, stratified grid turbulence. *Dyn. Atmos. Oceans* 23:155–69

Fjørtoft R. 1953. On the changes in the spectral distribution of kinetic energy for two-dimensional nondivergent flow. *Tellus* 5:225–30

Flór JB, van Heijst GJF. 1994. Experimental study of dipolar vortex structures in a stratified fluid. *J. Fluid Mech.* 279:101–34

Flór JB, van Heijst GJF. 1996. Stable and unstable monopolar vortices in a stratified fluid. *J. Fluid Mech.* 311:257–87

Flór JB, van Heijst GJF, Delfos R. 1995. Decay of dipolar vortex structures in a stratified fluid. *Phys. Fluids* 7:374–83

Fritts DC, Arendt S, Andreassen O. 1998. Vorticity dynamics in a breaking internal gravity wave. Part 2. Vortex interactions and transition to turbulence. *J. Fluid Mech.* 367:47–65

Gad-el-Hak M, Blackwelder RF, Riley JJ. 1981. On the growth of turbulent regions in laminar boundary layers. *J. Fluid Mech.* 110:73–95

Gage KS. 1979. Evidence for $\kappa^{5/3}$ power law range in mesoscale two-dimensional turbulence. *J. Atmos. Sci.* 43:729–39

Garrett CJR, Munk WH. 1979. Internal waves in the ocean. *Annu. Rev. Fluid Mech.* 11:339–69

Gerz T, Schumann U, Elghobashi SE. 1989. Direct numerical simulation of stratified homogeneous turbulent shear flows. *J. Fluid Mech.* 200:563–94

Gerz T, Yamazaki H. 1993. Direct numerical simulations of buoyancy driven turbulence in stably stratified fluid. *J. Fluid Mech.* 249:415–40

Gibson CH. 1980. Fossil temperature, salinity, and vorticity turbulence in the ocean. In *Marine Turbulence,* ed. JCJ Nihoul, pp. 221–57. New York; Elsevier

Gibson CH. 1987. Fossil turbulence and intermittancy in sampling oceanic mixing processes. *J. Geophys. Res.* 92:5383–404

Gilreath HE, Brandt A. 1985. Experiments on the generation of internal waves in a stratified fluid. *AIAA J.* 23:5

Godeferd FS, Cambon C. 1994. Detailed investigation of energy transfers in homogeneous stratified turbulence. *Phys. Fluids* 6:2084–100

Gregg MC. 1987. Diapycnal mixing in the thermocline: a review. *J. Geophys. Res.* 92:5249–86

Herring JR. 1980. Statistical theory of quasi-geostrophic turbulence. *J. Atmos. Sci.* 37:969–77

Herring JR, Métais O. 1989. Numerical experiments in forced stably stratified turbulence. *J. Fluid Mech.* 202:97–115

Holt SE, Koseff JR, Ferziger JH. 1992. A numerical study of the evolution and structure of homogeneous stably stratified sheared turbulence. *J. Fluid Mech.* 237:499–539

Hopfinger EJ. 1987. Turbulence in stratified fluids: a review. *J. Geophys. Res.* 92:5287–303

Hopfinger EJ, Flór JB, Chomaz JM, Bonneton P. 1991. Internal waves generated by a moving sphere and its wake in a stratified fluid. *Exp. Fluids* 11:255

Hopfinger EJ, Toly JA. 1976. Spatially decaying turbulence and its relation to mixing across density interfaces. *J. Fluid Mech.* 78:155–75

Huq P, Stretch DD. 1995. Critical dissipation rates in density stratified turbulence. *Phys. Fluids* 7:1034–39

Imberger J, Ivey GN. 1991. On the nature of turbulence in a stratified fluid. Part 2. Application to lakes. *J. Phys. Oceanogr.* 21:659–80

Itsweire EC, Helland KN. 1989. Spectra and energy transfer in stably stratified turbulence. *J. Fluid Mech.* 207:419–52

Itsweire EC, Helland KN, van Atta CW. 1986. The evolution of grid-generated turbulence in stably stratified fluid. *J. Fluid Mech.* 162:299–338

Ivey GN, Corcos GM. 1982. Boundary mixing in a stratified fluid. *J. Fluid Mech.* 121:1–26

Ivey GN, Imberger J. 1991. On the nature of turbulence in a stratified fluid. Part I. The energetics of mixing. *J. Phys. Oceanogr.* 21:650–58

Jacobitz FG, Sarkar S, van Atta CW. 1997. Direct numerical simulations of the turbulence evolution in a uniformly sheared and stably stratified flow. *J. Fluid Mech.* 342:231–61

Kaltenbach HJ, Schumann U, Gerz T. 1994. Large-eddy simulation of turbulent diffusion in a stably-stratified flow. *J. Fluid Mech.* 280:1–40

Kimura Y, Herring JR. 1996. Diffusion in stably-stratified turbulence. *J. Fluid Mech.* 328:253–69

Klostermeyer J. 1984. Two- and three-dimensional parametric instabilities in finite-amplitude internal gravity waves. *Geophys. Astrophys. Fluid Dyn.* 61:1–25

Kraichnan RH. 1967. Inertial ranges in two-dimensional turbulence. *Phys. Fluids* 10:1417–23

Kevorkian J, Cole JD. 1981. *Perturbation Methods in Applied Mathematics. Appl Math. Sci.* Vol. 34. Springer-Verlag

Kunze E. 1993. Submesoscale dynamics near a seamount. Part II: The partition of energy between internal waves and geostrophy. *J. Phys. Oceanogr.* 23:2589–601

Kunze E, Briscoe MG, Williams AJ III. 1990. Interpreting shear and strain finestructure from a neutrally buoyant float. *J. Geophys. Res.* 95:18127–42

Kunze E, Sanford TB. 1993. Submesoscale dynamics near a seamount. Part I: Measurement of Ertel vorticity. *J. Phys. Oceanogr.* 23:2567–88

Lamb H. 1932. *Hydrodynamics.* London: Cambridge Univ. Press

Lang RE. 1982. Decay of turbulence in stratified salt water. *J. Phys. Oceanogr.* 12:1508–14

Ledwell JR, Watson AJ, Law CS. 1993. Evidence of slow mixing across the pycnocline from an open-ocean tracer-release experiment. *Nature* 364:701–3

Leith CE. 1980. Nonlinear normal mode initialization and quasi-geostrophic theory. *J. Atmos. Sci.* 37:958–68

Lelong MP 1989. *Weakly-nonlinear internal wave/vortical mode interactions in stably-stratified flows.* PhD thesis. Univ. Wash., Seattle

Lelong MP, Dunkerton TJ. 1998a. Inertia-gravity wave breaking in three dimensions. Part I. Convectively stable waves. *J. Atmos. Sci.* 15:2473–88

Lelong MP, Dunkerton TJ. 1998b. Inertia-gravity wave breaking in three dimensions. Part II. Convectively unstable waves. *J. Atmos. Sci.* 15:2489–501

Lelong MP, McWilliams JC. 1999. Cyclostrophic adjustment in shallow-water and boussinesq fluids. *J. Fluid Mech.* In press

Lelong MP, Riley JJ. 1991. Internal wave–vortical mode interactions in strongly stratified flows. *J. Fluid Mech.* 232:1–19

Lesieur M, Métais O. 1996. New trends in large-eddy simulations of turbulence. *Annu. Rev. Fluid Mech.* 28:45–82

Lienhard JK, van Atta CW. 1990. The decay of turbulence in thermally stratified flow. *J. Fluid Mech.* 210:57–112

Lilly DK. 1973. Calculation of stably-stratified flow around complex terrain. *Flow Res. Note* No. 40

Lilly DK. 1983. Stratified turbulence and the mesoscale variability of the atmosphere. *J. Atmos. Sci.* 40:749–61

Lilly DK, Bassett G, Kroegemeier K, Bartello P. 1998. Stratified turbulence in the atmospheric mesoscales. *Theor. Comput. Fluid Dyn.* 11:139–54

Lin CL, Koseff JR, Ferziger JH. 1995. On triad interactions in a linearly stratified ocean. *J. Phys. Oceanogr.* 25:153–67

Lin JT, Pao YH. 1979. Wakes in stratified fluids: a review. *Annu. Rev. Fluid Mech.* 11:317–38

Lin Q, Lindberg WR, Boyer DL, Fernando HJS. 1992. Stratified flow past a sphere. *J. Fluid Mech.* 240:315–54

Lombard PN, Riley JJ. 1996a. Instability and breakdown of internal gravity waves. I. Linear stability analysis. *Phys. Fluids* 8:3271–87

Lombard PN, Riley JJ. 1996b. On the breakdown into turbulence of propagating internal waves. *Dyn. Atmos. Oceans* 23:345–55

Lorenz EN. 1960. Energy and numerical weather prediction. *Tellus* 12:364–77

Lorenz EN. 1980. Attractor sets and quasi-geostrophic equilibrium. *J. Atmos. Sci.* 37:1685–91

Lumley JL. 1964. The spectrum of nearly inertial turbulence in a stably stratified fluid. *J. Atmos. Sci.* 21:99–102

Mahrt L. 1998. Stratified atmospheric boundary layers and the breakdown of models. *Theor. Comp. Fluid Dyn.* 11:263–79

Majda AJ, Embid PF. 1998. Averaging over fast gravity waves for geophysical flows with unbalanced initial data. *Theoret. Comput. Fluid Dyn.* 11:155–69

Majda AJ, Grote MJ. 1997. Model dynamics and vertical collapse in decaying strongly stratified flows. *Phys. Fluids* 9(10):2932–40

Majda AJ, Grote MJ, Shefter MG. 1999. Analytical models for vertical collapse and instability in stably stratified flows. *Theoret. Comput. Fluid Dynam.* In press

Mason PJ, Derbyshire SH. 1990. Large-eddy simulation of the stably-stratified atmospheric boundary layer. *Bound. Layer Meteorol.* 53:117–62

McWilliams JC. 1980. An application of equivalent modons to atmospheric blocking. *Dyn. Atmos. Oceans* 5:43

McWilliams JC. 1985. A uniformly valid model spanning the regimes of geostrophic and isotropic, stratified turbulence: balanced turbulence. *J. Atmos. Sci.* 42:1773–74

McWilliams JC. 1988. Vortex generation through balanced adjustment. *J. Phys. Oceanogr.* 18:1178–92

Métais O, Herring JR. 1989. Numerical simulations of freely evolving turbulence in stably stratified fluids. *J. Fluid Mech.* 202:117–48

Métais O, Lesieur M. 1992. Spectral large-eddy simulations of isotropic and stably-stratified turbulence. *J. Fluid Mech.* 239:157–94

Métais O, Riley JJ, Lesieur M. 1994. Numerical simulations of stably-stratified rotating turbulence. In *Stably-Stratified Flows—Flow and Dispersion over Topography,* ed IP Castro, NJ Rockliff, Oxford, UK: Clarendon, pp. 139–51.

Mied RP. 1976. The occurrence of parametric instabilities in finite-amplitude internal gravity waves. *J. Fluid Mech.* 78:763–84

Milewski PA, Benney DJ. 1995. Resonant interactions between vortical flows and water waves. Part I. Deep water. *Stud. Appl. Math.* 94:131–67

Müller P, Holloway G, Henyey F, Pomphrey N. 1986. Nonlinear interactions among internal gravity waves. *Rev. Geophys.* 24:493–536

Müller P, Lien RC, Williams R. 1988. Estimates of potential vorticity at small scales in the ocean. *J. Phys. Ocean.* 18:401–16

Müller P, Olbers DJ, Willebrand J. 1978. The IWEX spectrum. *J. Geophys. Res.* 83:479–500

Orlanski I, Bryan K. 1969. Formation of thermocline step structure by large-amplitude internal gravity waves. *J. Geophys. Res.* 74:6975–83

Ozmidov RV. 1965. On the turbulent exchange in a stably stratified ocean. *Atmos. Ocean. Phys.* 1:493–97

Pao HP, Kao TW. 1977. Vortex structure in the wake of a sphere. *Phys. Fluids* 20:187–91

Park YG, Whitehead JA, Ghanadeskian A. 1994. Turbulent mixing in stratified fluids: layer formation and energetics. *J. Fluid Mech.* 279:279–311

Pearson HJ, Linden PF. 1983. The final stage of decay of turbulence in stably stratified fluid. *J. Fluid Mech.* 134:195–204

Pedlosky J. 1987. *Geophysical Fluid Dynamics.* New York: Springer-Verlag. 2nd edition

Phillips OM. 1960. On the dynamics of unsteady gravity waves of finite amplitude. Part 1. *J. Fluid Mech.* 9:193–217

Phillips OM. 1966. *The Dynamics of the Upper Ocean.* New York/London: Cambridge Univ. Press

Phillips OM. 1968. The interaction trapping of internal gravity waves. *J. Fluid Mech.* 34:407–16

Proudman J. 1916. On the motion of solids in a liquid possessing vorticity. *Proc. R. Soc.* A92:408–24

Ramsden D, Holloway G. 1992. Energy transfers across an internal wave-vortical mode spectrum. *J. Geophys. Res.* 97:3659–68

Riley JJ, Liu HT, Geller EW. 1976. A numerical model for stably stratified flow around complex terrain. In *Environmental Modeling and Simulation* (EPA 600/9-76-016), pp. 503–7

Riley JJ, Metcalfe RW, Weissman MA. 1981. Direct numerical simulations of homogeneous turbulence in density stratified fluids. In *Nonlinear Properties of Internal Waves,* ed. BJ West, pp. 79–112. Am. Inst. Physics

Rohr JJ, Itsweire EC, Helland KN, van Atta CW. 1988. Growth and decay of turbulence in a stably-stratified shear flow. *J. Fluid Mech.* 195:77–111

Rouhi A, Abarbanel HDI. 1991. Hamiltonian dynamics of coupled potential vorticity and internal wave motion. I. linear modes. *Geophys. Astrophys. Fluid Dyn.* 59:91–111

Siegel DA, Domaradzki. 1994. Large-eddy simulations of decaying, stably stratified turbulence. *J. Phys. Ocean.* 24:2353–86

Smith RB. 1989. Comment on "Low Froude number flow past three-dimensional obstacles. Part I. Baroclinically generated lee vortices." *J. Atmos. Sci.* 46:3611–13

Smolarkiewicz PK, Rotunno R. 1989. Low Froude number flow past three-dimensional obstacles. Part I. Baroclinically generated lee vortices. *J. Atmos. Sci.* 46:1154–64

Smyth WD, McWilliams JC. 1998. Instability of an axisymmetric vortex in a stably stratified, rotating environment. *Theoret. Comput. Fluid Dynamics.* 11:305–22

Spedding GR, Browand FK, Fincham AM. 1996a. The long-time evolution of the initially-turbulent wake of a sphere in a stable stratification. *Dyn. Atmos. Oceans* 23:171–82

Spedding GR, Browand FK, Fincham AM. 1996b. Turbulence, similarity scaling and vortex geometry in the wake of a towed sphere in a stably stratified fluid. *J. Fluid Mech.* 314:53–103

Staquet C. 1995. Two-dimensional secondary instabilities in a strongly stratified shear layer. *J. Fluid Mech.* 296:73–126

Staquet C, Riley JJ. 1989a. A numerical study of a stably-stratified mixing layer. In *Turbulent Shear Flows 6,* ed. J-C Andre, et al, pp. 381–97 Berlin, Heidelberg: Springer-Verlag

Staquet C, Riley JJ. 1989b. On the velocity field associated with potential vorticity. *Dyn. Atmos. Oceans.* 14:93–123

Stillinger DC, Helland KN, van Atta CW. 1983. Transition of homogeneous turbulence to internal waves in stratified fluid. *J. Fluid Mech.* 131:91–122

Sundermeyer MA. 1998. *Studies of lateral dispersion in the ocean.* PhD thesis. MIT/Woods Hole Joint Program in Physical Oceanography.

Taylor GI. 1923. Experiments on the motion of solid bodies in rotating fluids. *Proc. R. Soc.* A104:213–18

Thorpe SA. 1977. Turbulence and mixing in a Scottish loch. *Philos. Trans. R. Soc. London. Ser. A* 286:125–81

Thorpe SA. 1982. On the layers produced by rapidly oscillating a vertical grid in a uniformly stratified fluid. *J. Fluid Mech.* 124:391–409

Trieling RR, van Heijst GJF. 1998. Decay of monopolar vortices in a stratified fluid. *Fluid Dyn. Res.* 23:735–46

Turner JS. 1973. *Buoyancy Effects in Fluids.* New York/London: Cambridge Univ. Press

Vallis GK, Shutts GJ, Gray MEB. 1996. Balanced mesoscale motion and stratified turbulence forced by convection. *Q. J. R. Meterol. Soc.*, 123:1621–52

van Heijst GJF, Flór JB. 1989. Dipole formation and collisions in a stratified fluid. *Nature* 340:212

Van Zandt TE. 1982. A universal spectrum of buoyancy waves in the atmosphere. *Geophys. Res. Lett.* 9:575–78

Voropayev SI, Afanasyev YD, Filippov IA. 1991. Horizontal jet and vortex dipoles in a stratified medium. *J. Fluid Mech.* 227:543–66

Voropayev SI, Afanasyev YD, van Heijst GJF. 1995. Two-dimensional flows with zero net momentum: evolution of vortex quadrupoles and oscillating grid turbulence. *J. Fluid Mech.* 282:21–44

Voropayev SI, Zhang Z, Boyer DL, Fernando HJS, Pok CW. 1997. Horizontal jets in a rotating stratified fluid. *Phys. Fluids* 9:115–126

Warn T. 1986. Statistical mechanical equilibria of the shallow water equations. *Tellus* 38A:1–11

Werne J, Fritts DC. 1999. Stratified shear turbulence: evolution and statistics. *Geophys. Res. Lett.* 26(4):439–42

Winters KB, D'Asaro EA. 1994. Three-dimensional wave instability near a critical layer. *J. Fluid Mech.* 272:255–84

Yap CT, van Atta CW. 1993. Experimental studies of the development of quasi-two-dimensional turbulence in stably stratified fluid. *Dyn. Atmos. Oceans* 19:289–323

Yoon K, Warhaft Z. 1990. The evolution of grid generated turbulence under conditions of stable thermal stratification. *J. Fluid Mech.* 215:601–38